Global trends in marine nitrate N isotopes from observations and a neural network-based climatology

Patrick A. Rafter[1], Aaron Bagnell[2], Dario Marconi[3], and Timothy DeVries[2]

1: University of California, Irvine; 2 University of California, Santa Barbara; 3: Princeton University

Abstract

Nitrate is a critical ingredient for life in the ocean because, as the most abundant form of fixed nitrogen in the ocean, it is an essential nutrient for primary production. The availability of marine nitrate is principally determined by biological processes, each having a distinct influence on the N isotopic composition of nitrate (nitrate $\delta^{15}N$)—a property that informs much of our understanding of the marine N cycle as well as marine ecology, fisheries, and past ocean conditions. However, the sparse spatial distribution of nitrate $\delta^{15}N$ observations makes it difficult to apply this useful property in global studies, or to facilitate robust model-data comparisons. Here, we use a compilation of published nitrate $\delta^{15}N$ measurements (n = 12277) and climatological maps of physical and biogeochemical tracers to create a surface-to-seafloor, 1° resolution map of nitrate $\delta^{15}N$ using an Ensemble of Artificial Neural Networks (EANN). The strong correlation (R_2 > 0.87) and small mean difference (<0.05‰) between EANN-estimated and observed nitrate $\delta^{15}N$ indicates that the EANN provides a good estimate of climatological nitrate $\delta^{15}N$ without a significant bias. The magnitude of observation-model residuals is consistent with the magnitude of seasonal-decadal changes in observed nitrate $\delta^{15}N$ that are not captured by our climatological model. As such, these observation-constrained results provide a globally-resolved map of mean nitrate $\delta^{15}N$ for observational and modeling studies of marine biogeochemistry, paleoceanography, and marine ecology.

1 Introduction

In contrast to other marine nutrients (e.g., phosphate and silicate), the inventory of nitrate (NO_3^-) is mediated by biological processes, where the main source is N_2 fixation by diazotrophic phytoplankton and the main sink is denitrification (via a microbial consortium in oxygen deficient waters and sediments) (Codispoti and Christensen, 1985). Biological processes also determine the distribution of marine nitrate throughout the water column, with phytoplankton assimilating nitrate / lowering nitrate concentrations in the surface ocean and the microbially-mediated degradation of organic matter in the subsurface. (The latter involving the multi-step process of ammonification (organic matter → NH_4^+) and nitrification (NH_4^+ → NO_2^- → NO_3^-).) By regulating the global inventory and distribution of marine nitrate, these N cycling processes control global net primary productivity, the transfer of nutrients to higher trophic levels such as fishes, and the strength of the ocean's biological carbon pump (Dugdale and Goering, 1967).

Each of these biologically mediated N transformations affects the N isotopic composition of nitrate in unique ways (Fig.s 1A & 1B and see Section 2), adjusting the relative abundance of ^{15}N and ^{14}N in oceanic nitrate relative to the atmosphere. $\delta^{15}N$ = ($^{15}N/^{14}N$sample /

$^{15}N/^{14}N_{standard}$) – 1), multiplied by 1000 to give units of per mil (‰); see (Sigman and Casciotti, 2001) for simplified equations from (Mariotti et al., 1981). Nitrate $\delta^{15}N$ measurements have become a powerful tool for understanding the 'biogeochemical history' of marine nitrate, which includes nitrate assimilation by phytoplankton (Miyake and Wada, 1967; Wada and Hattori, 1978), nitrogen fixation (Carpenter et al., 1997; Hoering and Ford, 1960), denitrification (Liu, 1979), and nitrification (Casciotti et al., 2013). For example, the consumption of nitrate by denitrification (red line in Fig. 1A) has a larger impact on the residual nitrate $\delta^{15}N$ than does partial nitrate assimilation by phytoplankton (yellow line in Fig. 1), and thus very high $\delta^{15}N$ values serve as a fingerprint of denitrification. Nitrate $\delta^{15}N$ is also influenced by the addition of nitrate via remineralization of organic matter. The exact influence of remineralization depends on the isotopic composition of the organic matter, and could result in both higher or lower nitrate $\delta^{15}N$ (Fig. 1A). Nitrate introduced into the water column by the remineralization of organic matter formed by N_2-fixing phytoplankton has an isotopic composition close to that of air (0-1‰), and serves to lower the mean ocean $\delta^{15}N$ (Fig. 1B). On the other hand, organic matter formed from nitrate assimilation in regions where the plankton use most of the available nitrate can be isotopically heavy, and its remineralization will increase the $\delta^{15}N$ of ambient nitrate (Fig. 1B). The actual value of organic matter $\delta^{15}N$ formed from nitrate assimilation is mostly determined by: (1) the $\delta^{15}N$ of nitrate delivered to the euphotic zone (the subsurface source), which in turn is dependent on the degree of water-column denitrification and (2) the degree of nitrate consumption at the ocean surface, with heavier values associated with greater nitrate consumption (Fig. 1B). Accordingly, changes in organic matter $\delta^{15}N$ (and therefore sediment $\delta^{15}N$ used for paleoceanographic work) can reflect variability of the source nitrate $\delta^{15}N$ and/or variability of the degree of nitrate consumption (e.g., see (Rafter and Charles, 2012)).

Because of nitrate's place at the base of the marine ecosystem, nitrate $\delta^{15}N$ is also useful for understanding the lifecycles of higher trophic level organisms such as fish (Graham et al., 2007; Tawa et al., 2017) and fishery productivity (Finney et al., 2002, 2000). The $\delta^{15}N$ of whole sediment and microfossils provides insight *by proxy* of past ocean nitrate transformations (Altabet and Francois, 1994a; Kienast et al., 2008; Ren et al., 2009; Robinson et al., 2004; Sigman et al., 1999b)—work that places important constraints on modern ocean N cycling (Altabet, 2007; Eugster et al., 2013; Ren et al., 2017). With an understanding of the N transformations described above and their influences on the N isotopic composition of nitrate, we can begin using nitrate $\delta^{15}N$ measurements to trace the integrated biogeochemical history of marine nitrate. However, identifying basin- and global-scale trends in nitrate $\delta^{15}N$ is challenged by the limited spatial extent of nitrate $\delta^{15}N$ observations (Fig. 2). Here, we compile a global database of nitrate $\delta^{15}N$ measurements (Fig. 2) and use an Ensemble Artificial Neural Network (EANN) to produce a map of the global nitrate $\delta^{15}N$ distribution at 1-degree spatial resolution. We find that the mapped nitrate $\delta^{15}N$ climatology matches the observations well and should be a valuable tool for estimating mean conditions and for constraining predictive nitrate $\delta^{15}N$ models (Somes et al., 2010; Yang and Gruber, 2016). Below we briefly discuss how the EANN was used to produce global maps of nitrate $\delta^{15}N$ (Section 2), address the ability of the EANN to match

the measured $\delta^{15}N$ (Section 3), and examine the EANN-mapped $\delta^{15}N$ climatology and global compilation of nitrate $\delta^{15}N$ in the context of published work (Section 4).

2 Methods

2.1 Data Compilation

Nitrate $\delta^{15}N$ observations (Fig. 2; references in Table 3) were compiled from studies dating from 1975 (Cline and Kaplan, 1975) to 2018 (Fripiat et al., 2018), including data from the GEOTRACES Intermediate Data Product (Schlitzer et al., 2018). Whenever possible, the data was acquired via the original author, but in other cases the data was estimated from the publication directly. All observations were treated equally, although the failure to remove nitrite when using the "denitrifier method" may bias the nitrate $\delta^{15}N$ to low values (Rafter et al., 2013). These measurements have been identified as "nitrate+nitrite" in the dataset to acknowledge this potential biasing, which predominantly affects observations in the upper 100 m (Kemeny et al., 2016; Rafter et al., 2013).

2.2 Building the neural network model

We utilize an ensemble of artificial neural networks (EANNs) to interpolate our global ocean nitrate $\delta^{15}N$ database (Fig. 2), producing complete 3D maps of the data. By utilizing an artificial neural network (ANN), a machine learning approach that effectively identifies nonlinear relationships between a target variable (the isotopic dataset) and a set of input features (other available ocean datasets), we can fill holes in our data sampling coverage of nitrate $\delta^{15}N$.

2.2.1 Binning target variables (Step 1)

We binned the nitrate $\delta^{15}N$ observations (red symbols in Fig. 2) to the World Ocean Atlas 2009 (WOA09) grid with a 1-degree spatial resolution and 33 vertical depth layers (0-5500 m) (Garcia et al., 2010). When binning vertically, we use the depth layer whose value is closest to the observation's sampling depth (e.g. the first depth layer has a value of 0 m, the second of 10 m, and the third of 20 m, so all nitrate isotopic data sampled between 0-5 m fall in the 0 m bin; between 5-15 m they fall in the 10 m bin, etc.). An observation with a sampling depth that lies right at the midpoint between depth layers is binned to the shallower layer. If more than one raw data point falls in a grid cell we take the average of all those points as the value for that grid cell. Certain whole ship tracks of nitrate $\delta^{15}N$ data were withheld from binning to be used as an independent validation set (see section 2.2.4).

2.2.2 Obtaining input features (Step 2)

Our input dataset contains a set of climatological values for physical and biogeochemical ocean parameters that form a non-linear relationship with the target data. We have six input features including objectively analyzed annual-mean fields for temperature, salinity, nitrate, oxygen, and phosphate taken from the WOA09 (https://www.nodc.noaa.gov/OC5/WOA09/woa09data.html) at 1-degree resolution. Additionally, daily chlorophyll data from Modis Aqua for the period Jan-1-2003 through Dec-31-2012 is averaged and binned to the WOA09 grid (as described in Step 1) to produce an annual climatological field of chlorophyll values, which we then log transform to reduce their dynamic range.

The choice of these specific input features was dictated by our desire to achieve the best possible R^2 value on our internal validation sets (Step 4). Additional inputs besides those we included, such as latitude, longitude, silicate, euphotic depth, or sampling depth either did not improve the R^2 value on the validation dataset or degraded it, indicating that they are not essential parameters for characterizing this system globally. By opting to use the set of input features that yielded the best results for the global oceans, we potentially overlooked combinations of inputs that perform better at regional scales. However, given the scarcity of $\delta^{15}N$ data in some regions, it is not possible to ascribe the impact of a specific combination of input features versus the impact of available $\delta^{15}N$ data, which may not be representative of the region's climatological state, to the relative model performance in these regions.

2.2.3 Training the ANN (Step 3)

The architecture of our ANN consists of a single hidden layer, containing 25 nodes, that connects the biological and physical input features (discussed in Step 2) to the target nitrate isotopic variable (as discussed in Step 1). The role of the hidden layer is to transform input features into new features contained in the nodes. These are given to the output layer to estimate the target variable, introducing nonlinearities via an activation function. The number of nodes in this hidden layer, as well as the number of input features, determines the number of adjustable weights (the free parameters) in the network. Because there is a danger of over-fitting the model, which occurs when the ANN is over-trained on a dataset so that it cannot generalize well when presented with new data, it is a good practice to have a large number of training data (we have 7170 binned data points) relative to the number of weights (we have 201 free parameters) (Weigend et al., 1990). To create a nonlinear system, an activation function transforms the product of the weights and input features and creates the values assigned to nodes in the hidden layer. These act as new features for estimating the target $\delta^{15}N$ data. Our model utilizes the hyperbolic tangent as its activation function between the input and hidden layer as well as between the hidden and output layer due to its speed and general performance (Thimm and Fiesler, 1997).

The values of nodes in the hidden layer (H) can be defined as

$$H = a(I \cdot W_1 + b_1)$$

where H is an array containing the values of the hidden nodes, a is the activation function (here, the hyperbolic tangent), I is a 7170x6 array containing the values of the input features at the locations of the binned observations (there are 7170 binned observations and 6 input parameters), W_1 is a 6x25 array of weights that connect input features to hidden nodes, and b_1 is a 7170x25 array of weights (25 unique values repeated7170 times) that connects a bias node to the hidden nodes. The factor of 25 represents the number of nodes in the hidden layer, chosen by experimentation to find the maximum number of effective parameters (Foresee and Hagan 1997), i.e. where adding new parameters no longer improves performance on an internal validation set (Step 4). The bias node acts as

an offset term, similar to a constant term in a linear function, and has a value that is always 1.

At the output layer, the network produces a prediction of the target nitrate isotopic data ($\delta^{15}N_{pred}$). Similar to how nodes in the hidden layer are a function of the inputs and a set of weights, $\delta^{15}N_{pred}$ is a function of the hidden nodes and an additional set of weights. The predicted values can be defined as

$$d15N_{pred} = a(H \cdot W_2 + b_2)$$

where H (size 7170x25) has been previously defined, W_2 (size 25x1) is a matrix of weights that connect features in the hidden layer to nodes in the output layer, and b_2 (size 7170x1) is an array of weights (all of the same value) that connects a bias node to the output layer.

The ANN learns by comparing $\delta^{15}N_{pred}$ to the actual $\delta^{15}N$ data ($\delta^{15}N_{data}$), attempting to minimize the value of the cost function

$$\text{cost} = \frac{\sum_{i=1}^{n}(d15N_{pred}^{i} - d15N_{data}^{i})^2}{n}$$

by iteratively adjusting the weights using the Levenberg-Marquardt algorithm (Marquardt, 1963) as a way of propagating the errors between $\delta^{15}N_{pred}$ and $\delta^{15}N_{data}$ backwards though the network (Rumelhart et al., 1986).

2.2.4 Validating the ANN (Step 4)

To ensure good generalization of the trained ANN, we randomly withhold 10% of the $\delta^{15}N$ data to be used as an internal validation set for each network. This is data that the network never sees, meaning it does not factor into the cost function, so it works as a test of the ANN's ability to generalize. This internal validation set acts as a gatekeeper to prevent poor models from being accepted into the ensemble of trained networks (see Step 5). A second, independent or 'external' validation set (blue symbols in Fig. 2), composed of complete ship transects from the high and low latitude ocean were omitted from binning in Step 1 and used to establish the performance of the entire ensemble. Our rationale for using complete ship transects is the following. If we randomly chose 10% of observations to perform an external validation, this dataset will be from the same cruises as the wider data. In other words, despite being randomly selected, the validating observational dataset will be highly correlated geographically. Contrast this with validating the EANN results with observations from whole research cruises in unique geographic regions—areas where the model has not "learned" anything about nitrate. We therefore argue that these observations from whole ship tracks therefore provide a more difficult test of the model.

2.2.5 Forming the Ensemble (Step 5)

The ensemble is formed by repeating Steps 3 to 4 (using a different random 10% validation set) until we obtain 25 trained networks for the nitrate $\delta^{15}N$ dataset. A network is admitted into the ensemble if it yields an R^2 value greater than 0.81 on the validation dataset. Using

an EANN instead of any single network provides several advantages. For example, the random initialization of the weight values in each network as well as differences in the training and internal validation sets used across members make it possible for many different networks to achieve similar performance on their respective validation set while generalizing to areas with no data coverage differently. By performing this type of data subsampling and taking an ensemble average, similar to bootstrap aggregating (Breiman, 1996) this approach on average improves the robustness of the generalization in areas without data coverage compared to a single randomly generated ensemble member. Compared to each of its members, our ensemble mean sees improved performance on all internal validation sets and has a higher R^2 and lower root mean square error on the independent validation set compared to 19 of the 25 members. The range of values given by the ensemble also provides a measure of the uncertainty for our estimations of $\delta^{15}N$.

3 Results

3.1 Global nitrate $\delta^{15}N$ observations

The global compilation of nitrate $\delta^{15}N$ includes 1180 stations from all major ocean basins and some minor seas (Fig. 2) giving a total of 12277 nitrate $\delta^{15}N$ measurements. Within this dataset, 1197 nitrate $\delta^{15}N$ measurements were withheld from the EANN and used to validate the EANN results to ensure good extrapolation (the 'external' validation dataset; blue symbols in Fig. 2, see Section 2). With observations from the surface to as deep as 6002 m (Rafter et al., 2012), we find that nitrate $\delta^{15}N$ ranges from ≈1‰ in the North Atlantic (e.g., Marconi et al., (2015)) to 68.7‰ in the Eastern Tropical South Pacific (Bourbonnais et al., 2015). Nitrate $\delta^{15}N$ of ≈1‰ was also irregularly observed in the shallow North and South Pacific (Liu et al., 1996; Yoshikawa et al., 2015). These latter observations were included in the training dataset, although we should note that the measurements using the 'Devarda's Alloy' method (Liu et al., 1996) is thought to be biased low (Altabet and Francois, 2001). Similarly, the inclusion of nitrite for 'denitrifier method' nitrate $\delta^{15}N$ can bias the measurement to lower values (Kemeny et al., 2016; Rafter et al., 2013).

3.2 Marine nitrate $\delta^{15}N$ observations-model comparison

The observed and EANN-predicted nitrate $\delta^{15}N$ measurements are distributed around a 1:1 line in Fig. 3A (all data), with considerably less scatter for the deeper values (data >1000 m; Fig. 3B). The correlation coefficient of determination for the observations versus the model nitrate $\delta^{15}N$ gives an R^2=0.75 for the raw / unbinned observations used to train the EANN and an R^2 of 0.78 for the validation dataset. We can also examine the performance of the EANN with the nitrate $\delta^{15}N$ "residual" or the difference between observed and modeled $\delta^{15}N$, which indicates a mean residual or 'mean bias' value of -0.03‰ for the entire dataset and +0.18‰ for the validation dataset.

Examining the observation-EANN residuals via the Root Mean Square Error (RMSE), we find an RMSE of 1.94‰ for the data used to train the EANN and an RMSE of 1.26‰ for the external validation dataset. There is a clear relationship between RMSE and depth, with a significantly higher RMSE for the upper 500 m (Figs. 3C and 3D). Comparing these residual values with dissolved oxygen concentrations (color in Fig. 3C), we find that >2‰ RMSE for

the surface is associated with high oxygen while >2.7‰ RMSE at ≈250 m is associated with the lowest oxygen. Furthermore, the RMSE of the observation-EANN residuals differs between the datasets used to train the model (solid red line in Fig. 3D) and validate the model (dashed line in Fig. 3D).

The RMSE patterns in Figs. 3C and 3D are to be expected given the natural variability in nitrate δ^{15}N driven by assimilation in the upper ocean and denitrification in the shallow sub-surface—variability which is not captured by the climatological EANN. Rafter and Sigman, (2016), presented a 5-year time-series of nitrate δ^{15}N from the eastern equatorial Pacific, which showed that variability of nitrate assimilation produces seasonal-to-interannual deviations of δ^{15}N of ±2.5‰, which is similar to the magnitude of the RMSE in the surface ocean (2.2‰). Although there are no nitrate δ^{15}N time-series measurements from the subsurface Oxygen Deficient Zone (ODZ) waters where denitrification occurs, nitrate δ^{15}N in ODZs presumably have similar seasonal-to-interannual (or longer timescale) variability due to changes in the rate and extent of water column denitrification (Deutsch et al., 2011; Yang et al., 2017). For example, a larger degree of nitrate undergoing water column denitrification would explain the extreme δ^{15}N values at the bottom right of Fig. 3A—observations that all come from the ODZ waters of the Eastern Tropical South Pacific (Bourbonnais et al., 2015; Casciotti et al., 2013; Rafter et al., 2012; Ryabenko et al., 2012). Some of these very high nitrate δ^{15}N values are associated with nitrate concentrations <1 μmol kg^{-1} (Bourbonnais et al., 2015), values much lower than within our climatology for the subsurface Eastern Tropical South Pacific. These values thus represent episodic denitrification events that the EANN will not be able to capture because it is trained on climatological data. In the deep ocean where temporal variability is smaller, the observation-EANN residuals of 0.2‰ are the same magnitude as the δ^{15}N analytical errors, further emphasizing the ability of the model to match climatological average conditions.

4 Discussion

The EANN's skillful estimate of climatological nitrate δ^{15}N will be useful for studies of the marine nitrogen cycle. The zonal average view of EANN nitrate δ^{15}N for each major ocean basin (Fig. 4) includes statistics comparing the observations versus EANN results above and below 1000 m. These region-specific statistics show a weaker correlation between EANN and observed nitrate δ^{15}N in the deep Atlantic and Southern Ocean, despite low RMSE and negligible mean bias. This weak correlation likely derives from the limited variability of deep nitrate δ^{15}N (±0.1‰) in these basins (see Fig. 5D).

The nitrate δ^{15}N sections in Fig. 4 show elevated values for the low latitude, upper mesopelagic Pacific (Fig. 4A) and Indian Oceans (Fig. 4D) where water column denitrification raises the residual nitrate δ^{15}N (Fig. 1A). Viewing this elevated nitrate δ^{15}N at the 250 m depth horizon (Fig. 5) better reveals the spatial heterogeneity of the observations and EANN results. (It is because of this intra-basin heterogeneity, and the fact that many observations are biased towards the areas of denitrification, that we did not plot the observed nitrate δ^{15}N within the zonally-averaged Fig. 4 views.) The EANN error for the Fig. 5 depth intervals (Figs. 5E-5H) is the standard deviation of the 25 ensemble members of the EANN and shows a decrease in ensemble variability with depth—a trend that is

consistent with the overall decrease in observed nitrate $\delta^{15}N$ variability with depth (Figs. 4 & 5).

Below we inspect the observed and EANN-predicted nitrate $\delta^{15}N$ and discuss the consistency of these results with our understanding of published work. This analysis begins with the spatial distribution of nitrate delivered to the upper ocean. We then discuss the impacts of upper ocean nitrate assimilation on organic matter $\delta^{15}N$ and consider the influence of organic matter remineralization on sub-surface nitrate.

4.1 Subsurface and surface nitrate $\delta^{15}N$

The nitrate $\delta^{15}N$ distribution at 250 m depth (Fig. 5B) offers a view of nitrate at a depth that is deeper than source waters in many ocean regions (e.g., 100 to 150 m in the equatorial Pacific (Rafter and Sigman, 2016)), but is negligibly influenced by nitrate assimilation, and therefore provides a qualitative view of spatial trends in nitrate delivered to the surface ocean. Nitrate $\delta^{15}N$ at this depth is highest in the North and South Eastern Tropical Pacific and Arabian Seas (Fig. 5B), due to the influence of water column denitrification in the ODZs in these regions (Altabet et al., 2012; Bourbonnais et al., 2015; Ryabenko et al., 2012), which preferentially uses the light isotope and leaves the residual nitrate enriched in ^{15}N. A notable difference between the EANN and a previous biogeochemical model estimate of nitrate $\delta^{15}N$ (Somes et al., 2010) is that the EANN correctly captures the higher nitrate $\delta^{15}N$ in the Arabian Sea compared to the Bay of Bengal.

Lowest $\delta^{15}N$ values of sub-surface nitrate are found in the Southern Ocean and in the North Atlantic. The North Atlantic subtropical gyre in particular has the lowest $\delta^{15}N$ values in any basin (Fig. 5B; also see (Fawcett et al., 2011; Knapp et al., 2005, 2008)), which can be attributed to the remineralization of low-$\delta^{15}N$ organic matter originating from N_2-fixation, which produces organic matter with a $\delta^{15}N$ between 0 and -1‰ (similar to atmospheric N_2; see Fig. 1B (Carpenter et al., 1997; Hoering and Ford, 1960)). Prior work argues that this nitrate $\delta^{15}N$ lowering requires the bulk of Atlantic N_2-fixation (≈90%) to occur in the tropics (Marconi et al., 2017) followed by the advection of remineralized nitrate to the North Atlantic. This contrasts with numerical models arguing for high N_2-fixation rates in the North Atlantic (Ko et al., 2018). Similar local minima of sub-surface $\delta^{15}N$ appear in all the sub-tropical gyres (Fig. 5B), which is consistent with observations (Casciotti et al., 2008; Yoshikawa et al., 2015) and presumably indicates the importance of N_2-fixation in these regions (Ko et al., (2018) and others). The N_2-fixation $\delta^{15}N$ signal in the Pacific Ocean is counteracted by the influence of water-column denitrification in that basin, which imparts a high $\delta^{15}N$ signal, but a local minimum in $\delta^{15}N$ can still be seen in the Pacific subtropical gyres (Fig. 4A).

Nitrate assimilation by phytoplankton in the upper ocean is influenced by both the subsurface source nitrate $\delta^{15}N$ and the degree of nitrate assimilation (Miyake and Wada, 1967; Wada and Hattori, 1978) (Fig. 1B). This gives the expectation that average nitrate $\delta^{15}N$ values for the upper 50 m (Fig. 5A) will be consistently higher than those at 250 m (Fig. 5B). However, the highest values in the upper 50 m are not found above the ODZ

regions, but are on the edges of high nitrate concentration upwelling zones in the Southern Ocean, equatorial Pacific, and subarctic gyres (contours in Fig. 2). Circulation in these 'edge' regions allows for nitrate to be advected along the surface, lengthening its time in the surface ocean and allowing more utilization to elevate the residual nitrate $\delta^{15}N$ pool. In other words, the degree of nitrate utilization appears to play a more important role in determining surface nitrate $\delta^{15}N$ than the initial value. (This is not the case for the organic matter $\delta^{15}N$ produced from this nitrate, which will be discussed more below.)

Despite our expectation of higher nitrate $\delta^{15}N$ in the upper 50 m versus 250 m (Figs. 5A vs. 5B), we identify two types of regions where this difference is negative (Fig. 6): above ODZ waters and in subtropical gyres. The explanation for the negative values above the ODZ regions is that the nitrate $\delta^{15}N$ at 250 m must be much higher than the nitrate $\delta^{15}N$ upwelled to the surface. This is consistent with elevated ODZ nitrate $\delta^{15}N$ having an indirect path to waters outside of ODZ regions (Peters et al., 2017; Rafter et al., 2013). The subtropical gyres also have modeled nitrate $\delta^{15}N$ in the upper 50 m that is less than 250 m, but this finding is difficult to test with observations because of low nitrate concentrations. That said, the model predicts a lower nitrate $\delta^{15}N$ in the upper ocean relative to that at 250 m, which is consistent with N_2-fixation in these regions.

Our discussion above highlights the difficulty of distinguishing between the competing influences of the subsurface source nitrate $\delta^{15}N$ and the degree of nitrate utilization on residual nitrate $\delta^{15}N$. Clearly a static depth does not reflect the subsurface source of nitrate delivered to the surface and a more robust method for estimating this subsurface source needs to be developed. However, some generalizations can be made regarding the organic matter $\delta^{15}N$ produced in these regions and its potential influence (via remineralization) on subsurface nitrate throughout the water column via the export and remineralization of organic matter (Sigman et al., 2009a). For example, a local minimum in $\delta^{15}N$ is visible at 250 m depth in the Eastern Equatorial Pacific (Fig. 5B; also discussed in several studies (Rafter et al., 2012; Rafter and Sigman, 2016)) is caused by the remineralization of organic matter with a low $\delta^{15}N$ due to partial nitrate consumption at the surface. Below we discuss these and other influences on intermediate-depth nitrate $\delta^{15}N$.

4.2 Intermediate-depth nitrate $\delta^{15}N$ variability

Waters at "intermediate" depths (here shown as the 750 m surface in Fig. 5C) are important because they are part of a large-scale circulation that initially upwells in the Southern Ocean and ultimately resupplies nutrients to the low latitude thermocline (Palter et al., 2010; Sarmiento et al., 2004; Toggweiler et al., 1991; Toggweiler and Carson, 1995). Within the context of this overturning, the nitrate upwelling in the Southern Ocean is initially ≈5‰ (Figs. 4C & 5C) and the $\delta^{15}N$ is elevated ≈2‰ by partial nitrate assimilation in surface waters as they are advected equatorward (see Figs. 5A and 6). Deep wintertime mixing in the Subantarctic Pacific converts these surface waters into mode and intermediate waters (Herraiz-Borreguero and Rintoul, 2011), introducing nitrate with a "pre-formed" $\delta^{15}N$ of ≈6‰ into the intermediate-depth South Pacific and South Atlantic (Rafter et al., 2012, 2013; Tuerena et al., 2015) at depths between ≈600-1200 m. The

399 penetration of this pre-formed signal (nitrate ≥ 6‰) into the interior can be clearly seen in
400 the Atlantic Ocean between ≈40°S to 20°N (Fig. 4B).
401
402 The same signal is carried with Southern Ocean mode and intermediate waters into the
403 Pacific basin as far as the tropics (Lehmann et al., 2018; Rafter et al., 2013), although it is
404 difficult to distinguish in the model results against the higher background $\delta^{15}N$ in this
405 basins (Figs. 4A, 4D, 5C). The same process presumably introduces elevated nitrate $\delta^{15}N$ to
406 the Indian Ocean, which has similar values at this depth. Nitrate $\delta^{15}N$ increases from the
407 Southern Ocean toward the equator in the Pacific and Indian Oceans, but not in the Atlantic
408 (Fig. 5C). Organic matter has a lower $\delta^{15}N$ in the Atlantic than in the Pacific and Indian
409 because of a lack of water-column denitrification supplying high-$\delta^{15}N$ water to the surface,
410 and because of the high rates of N_2-fixation which supply isotopically light N to organic
411 matter (Marconi et al., 2017; Tuerena et al., 2015). This contrast in intermediate-depth
412 nitrate $\delta^{15}N$ can be traced to the lower $\delta^{15}N$ of organic matter remineralized in this
413 region—an explanation that is also consistent with enhanced N_2 fixation in the tropical
414 Atlantic (Marconi et al., 2017). The increase in intermediate-depth nitrate $\delta^{15}N$ from the
415 Subantarctic to the tropical Pacific appears to result from the remineralization of organic
416 matter with a $\delta^{15}N$ elevated by high source nitrate $\delta^{15}N$ (near the ODZ) or extreme
417 elevation of residual nitrate $\delta^{15}N$ (advected along the surface away from the equator; see
418 high surface nitrate $\delta^{15}N$ in Fig. 5A). Previous work suggests that direct mixing with
419 denitrified waters represents only a small fraction of the change from the pre-formed high
420 latitude value (≈6‰) to tropical nitrate $\delta^{15}N$ of ≈7‰ (Peters et al., 2017; Rafter et al.,
421 2012, 2013).
422
423 The South Indian Ocean is one region particularly devoid of published nitrate $\delta^{15}N$
424 observations (Fig. 2), but the EANN makes specific predictions about its distribution. For
425 example, the modeled nitrate $\delta^{15}N$ predicts that intermediate-depth Indian Ocean nitrate is
426 similarly elevated in $\delta^{15}N$ to the intermediate-depth South Pacific (Fig. 5C). Considering
427 that both intermediate-depth water masses are formed from Southern Ocean surface
428 waters, it is reasonable to propose that nitrate $\delta^{15}N$ are similarly elevated by partial nitrate
429 consumption. The EANN therefore provides testable predictions for nitrate $\delta^{15}N$
430 observations throughout the Indian Ocean.
431
432 **4.4 Deep-sea nitrate $\delta^{15}N$ trends**
433 Our discussion above suggests that the basin-scale balance of N_2-fixation and water-column
434 denitrification is a major contributor to inter-basin nitrate $\delta^{15}N$ gradients in the upper
435 ocean, lowering values in the Atlantic Oceans compared to the Pacific and Indian Oceans.
436 Averaging EANN nitrate $\delta^{15}N$ with depth for each ocean basin (Fig. 7), we find that these
437 basin-scale nitrate $\delta^{15}N$ differences also persist into the deep-sea (here defined as 3000 m
438 and below). (Note that the inter-basin EANN nitrate $\delta^{15}N$ gradients in Fig. 7 are smaller
439 than the corresponding inter-basin gradients in observed $\delta^{15}N$, because the observations
440 are spatially biased towards areas of water column denitrification in the Pacific and Indian
441 Oceans (see Fig. 2).)
442

The remineralization of organic matter is one process that can—and has been used to—explain both the elevation of deep Pacific nitrate δ^{15}N (Peters et al., 2017; Rafter et al., 2013; Sigman et al., 2009a)(Peters et al., 2017; Rafter et al., 2013; Sigman et al., 2009) and lowering of deep Atlantic nitrate δ^{15}N (Knapp et al., 2008; Marconi et al., 2017; Tuerena et al., 2015) relative to the deep ocean mean. Here we provide two additional pieces of evidence that argue for the remineralization of organic matter as the key driver of these deep-sea nitrate δ^{15}N differences. Our first piece of evidence is that the average subsurface source of nitrate to the Pacific and Indian Ocean surface has a significantly higher δ^{15}N (by 2‰ at the 250 m depth surface) than the Atlantic and Southern Oceans (Figs. 5B and 7). Nitrate δ^{15}N at 250 m is an admittedly imprecise estimate for the nitrate upwelled to the surface, but even a slight elevation in Pacific source nitrate δ^{15}N and near complete nitrate utilization at the surface will translate into higher sinking organic matter δ^{15}N (i.e., see Fig. 1B).

Our second piece of evidence that the export and remineralization of organic matter drives the inter-basin differences in deep nitrate δ^{15}N comes from sediment trap measurements. Averaging published sediment trap organic matter δ^{15}N from the subtropical and tropical Pacific gives a value of 8.5±2.9‰ (Knapp et al., 2016; Robinson et al., 2012), which is significantly higher than measured in traps from the Atlantic (4.5±1.5‰) (Freudenthal et al., 2001; Holmes et al., 2002; Lavik, 2000; Thunell et al., 2004). Given observed Southern Ocean nitrate characteristics (Rafter et al., 2013), we estimate an even lower typical sinking organic matter δ^{15}N of +1.5‰ for this region, which assumes initial nitrate values equal the Upper Circumpolar Deep Water and final values from the Open Antarctic Zone. This value is consistent with annually-averaged sinking organic matter δ^{15}N of ≈0.9 to 1.6‰ (Lourey et al., 2003), although published results from the iron-fertilized Kerguelen Plateau region are predictably higher (Trull et al., 2008). The much lower Southern Ocean sinking organic matter δ^{15}N is consistent with partial consumption of nitrate at the surface (see Fig. 1B) and the entrainment of this nitrate in equatorward-moving intermediate waters acts to export nitrate with elevated δ^{15}N to intermediate waters throughout the Southern Hemisphere (see discussion above). Based on this evidence, it appears that global patterns of sinking organic matter δ^{15}N are consistent with the remineralization of this organic matter driving subtle, but significant differences in deep-sea nitrate δ^{15}N.

An alternative explanation for the deep-sea nitrate δ^{15}N differences in Fig. 7 is that they reflect the lateral (along isopycnal) advection of elevated nitrate δ^{15}N from ODZ regions. However, we can easily dismiss this explanation by looking at the meridional trends in deep-sea nitrate δ^{15}N—following the deep waters from their entrance in the south and movement northward. What we find is that deep EANN nitrate δ^{15}N (Fig. 5D) is lowest in the Southern Ocean and increases equatorward in the Pacific. Average observed nitrate δ^{15}N below 2500 m increases from 4.7±0.1‰ in the Pacific sector of the Southern Ocean to 4.9±0.2‰ in the deep South Pacific, 5.4±0.2‰ in the deep tropical Pacific, and 5.2±0.2‰ in the deep North Pacific. This is consistent with the known increase in nitrate concentrations and lowering of deep oxygen concentrations from the deep South to Tropical and North Pacific (e.g., see Fig. 4E in (Rafter et al., 2013)). This contrasts with no significant change in deep Atlantic nitrate δ^{15}N, despite the export of slightly elevated

nitrate $\delta^{15}N$ into intermediate-depth Atlantic (see above and (Tuerena et al., 2015)) and the introduction of a different deep water mass (North Atlantic Deep Water) in the North Atlantic. The distribution of deep Pacific nitrate $\delta^{15}N$ is coherent with elevated organic matter $\delta^{15}N$ being produced and exported from the lower latitude surface and remineralized at depth. In other words, inter-basin differences sinking organic matter $\delta^{15}N$ best explains the inter-basin differences in deep EANN and observed nitrate $\delta^{15}N$. Diapycnal mixing from the low latitude Pacific ODZ regions may also play a role in the south-to-north elevation of deep Pacific nitrate $\delta^{15}N$, but we cannot quantify the magnitude of that influence without a circulation model. Future work should look into this issue.

5 Conclusions

We find that an Ensemble of Artificial Neural Networks (EANN) can be trained on climatological distributions of physical and biogeochemical tracers to reproduce a global database of nitrate $\delta^{15}N$ observations (Fig. 2) with good fidelity (Fig. 3). We used the EANN to produce global climatological maps of nitrate $\delta^{15}N$ at a 1 degree-resolution from the surface to the seafloor. These results help identify spatial patterns (Figs. 4-6) and quantify regional and basin-average oceanic values of nitrate $\delta^{15}N$ (Fig. 7). Major differences between the observed and EANN-predicted nitrate $\delta^{15}N$ appear to be caused by temporal variability of nitrate $\delta^{15}N$ in the upper ocean and in ODZs associated with variable nitrate uptake and denitrification rates. Additional measurements of nitrate $\delta^{15}N$ will help to develop seasonally-resolved maps that can improve upon the climatological mean map provided here.

Acknowledgments: M. Altabet, K. Casciotti, A. Santoro, B. Pasquier, J. J. Becker, two anonymous reviewers and M. Kienast, as well as J. Granger and D. M. Sigman for (at-the-time) unpublished data. A complete list of references can be found in the Appendix. The compiled data set and data product is available in several online databases (BCO-DMO.org, pangaea.de, and webodv.awi.de). Many figures were made using Ocean Data View software (Schlitzer, 2002). Custom made color palettes and are available via www.prafter.com.

References

Altabet, M. A.: Constraints on oceanic N balance/imbalance from sedimentary N-15 records, Biogeosciences, 4(1), 75–86, 2007.

Altabet, M. A. and Francois, R.: Sedimentary nitrogen isotopic ratio as a recorder for surface ocean nitrate utilization, Glob. Biogeochem. Cycles, 8(1), 103–116, 1994a.

Altabet, M. A. and Francois, R.: The use of nitrogen isotopic ratio for reconstruction of past changes in surface ocean nutrient utilization, in Carbon Cycling in the Glacial Ocean: Constraints on the Ocean's Role in Global Change, vol. 117, pp. 281–306, Springer-Verlag Berlin Heidelberg., 1994b.

Altabet, M. A. and Francois, R.: Nitrogen isotope biogeochemistry of the antarctic polar frontal zone at 170 degrees W, Deep-Sea Res. Part Ii-Top. Stud. Oceanogr., 48(19–20), 4247–4273, 2001.

Altabet, M. A., Murray, D. W. and Prell, W. L.: Climatically linked oscillations in Arabian Sea denitrification over the past 1m.y.: Implications for the marine N cycle, Paleoceanography, 14(6), 732–743, 1999.

Altabet, M. A., Ryabenko, E., Stramma, L., Wallace, D. W. R., Frank, M., Grasse, P. and Lavik, G.: An eddy-stimulated hotspot for fixed nitrogen-loss from the Peru oxygen minimum zone, Biogeosciences, 9(12), 4897–4908, doi:10.5194/bg-9-4897-2012, 2012.

Altabet, M. A., Pilskaln, C. .. Thunell, R. .. Pride, C. .. Sigman, D. .. Chavez, F. .. Francois, R.: The nitrogen isotope biogeochemistry of sinking particles from the margin of the Eastern North Pacific, Deep-Sea Res. Part -Oceanogr. Res. Pap., 46(4), 655–679, 1999.

Bourbonnais, A., Lehmann, M. F., Waniek, J. J. and Schulz-Bull, D. E.: Nitrate isotope anomalies reflect N_2 fixation in the Azores Front region (subtropical NE Atlantic), J. Geophys. Res., 114(C3), doi:10.1029/2007JC004617, 2009.

Bourbonnais, A., Altabet, M. A., Charoenpong, C. N., Larkum, J., Hu, H., Bange, H. W. and Stramma, L.: N-loss isotope effects in the Peru oxygen minimum zone studied using a mesoscale eddy as a natural tracer experiment, Glob. Biogeochem. Cycles, 29(6), 793–811, doi:10.1002/2014GB005001, 2015.

Brandes, J. A., Devol, A. H., Yoshinari, T., Jayakumar, D. A. and Naqvi, S. W. A.: Isotopic composition of nitrate in the central Arabian Sea and eastern tropical North Pacific: A tracer for mixing and nitrogen cycles, Limnol. Oceanogr., 43(7), 1680–1689, 1998.

Breiman, L.: Bagging predictors, Mach. Learn., 24(2), 123–140, doi:10.1007/BF00058655, 1996.

Carpenter, E. J., Harvey, H. R., Fry, B. and Capone, D. G.: Biogeochemical tracers of the marine cyanobacterium Trichodesmium, Deep-Sea Res. Part -Oceanogr. Res. Pap., 44(1), 27–38, doi:10.1016/s0967-0637(96)00091-x, 1997.

554 Casciotti, K. L. and McIlvin, M. R.: Isotopic analyses of nitrate and nitrite from reference
555 mixtures and application to Eastern Tropical North Pacific waters, Mar. Chem., 107(2),
556 184–201, doi:10.1016/j.marchem.2007.06.021, 2007.

557 Casciotti, K. L., Trull, T. W., Glover, D. M. and Davies, D.: Constraints on nitrogen cycling at
558 the subtropical North Pacific Station ALOHA from isotopic measurements of nitrate and
559 particulate nitrogen, Deep-Sea Res. Part Ii-Top. Stud. Oceanogr., 55(14–15), 1661–1672,
560 doi:10.1016/j.dsr2.2008.04.017, 2008.

561 Casciotti, K. L., Buchwald, C. and McIlvin, M.: Implications of nitrate and nitrite isotopic
562 measurements for the mechanisms of nitrogen cycling in the Peru oxygen deficient zone,
563 Deep Sea Res. Part Oceanogr. Res. Pap., 80, 78–93, doi:10.1016/j.dsr.2013.05.017, 2013.

564 Cline, J. D. and Kaplan, I. R.: Isotopic fractionation of dissolved nitrate during denitrification
565 in the eastern tropical North Pacific Ocean, Mar. Chem., 3(4), 271–299, doi:10.1016/0304-
566 4203(75)90009-2, 1975.

567 Codispoti, L. . and Christensen, J. .: Nitrification, denitrification and nitrous oxide cycling in
568 the eastern tropical South Pacific ocean, Mar. Chem., 16(4), 277–300, doi:10.1016/0304-
569 4203(85)90051-9, 1985.

570 De Pol-Holz, R., Robinson, R. S., Hebbeln, D., Sigman, D. M. and Ulloa, O.: Controls on
571 sedimentary nitrogen isotopes along the Chile margin, Deep-Sea Res. Part II-Top. Stud.
572 Oceanogr., 56(16), 1100–1112, doi:10.1016/j.dsr2.2008.09.014, 2009.

573 Dehairs, F., Fripiat, F., Cavagna, A.-J., Trull, T. W., Fernandez, C., Davies, D., Roukaerts, A.,
574 Fonseca Batista, D., Planchon, F. and Elskens, M.: Nitrogen cycling in the Southern Ocean
575 Kerguelen Plateau area: evidence for significant surface nitrification from nitrate isotopic
576 compositions, Biogeosciences, 12(5), 1459–1482, doi:10.5194/bg-12-1459-2015, 2015.

577 Deutsch, C., Brix, H., Ito, T., Frenzel, H. and Thompson, L.: Climate-Forced Variability of
578 Ocean Hypoxia, Science, 333(6040), 336–339, doi:10.1126/science.1202422, 2011.

579 DeVries, T., Deutsch, C., Rafter, P. A. and Primeau, F.: Marine denitrification rates
580 determined from a global 3-dimensional inverse model, Biogeosciences Discuss., 9(10),
581 14013–14052, doi:10.5194/bgd-9-14013-2012, 2012.

582 DiFiore, P. J., Sigman, D. M., Trull, T. W., Lourey, M. J., Karsh, K., Cane, G. and Ho, R.: Nitrogen
583 isotope constraints on subantarctic biogeochemistry, J. Geophys. Res.-Oceans, 111(C8),
584 doi:10.1029/2005jc003216, 2006.

585 Dugdale, R. C. and Goering, J. J.: Uptake of new and regenerated forms of nitrogen in
586 primary production, Limnol. Oceanogr., 12(2), 196–206, 1967.

587 Eugster, O., Gruber, N., Deutsch, C., Jaccard, S. L. and Payne, M. R.: The dynamics of the
588 marine nitrogen cycle across the last deglaciation, Paleoceanography, 28(1), 116–129,
589 doi:10.1002/palo.20020, 2013.

590 Fawcett, S. E., Lomas, M., Casey, J. R., Ward, B. B. and Sigman, D. M.: Assimilation of upwelled
591 nitrate by small eukaryotes in the Sargasso Sea, Nat. Geosci., 4(10), 717–722,
592 doi:10.1038/ngeo1265, 2011.

593 Finney, B. P., Gregory-Eaves, I., Douglas, M. S. V. and Smol, J. P.: Fisheries productivity in the
594 northeastern Pacific Ocean over the past 2,200 years, Nature, 416(6882), 729–733,
595 doi:10.1038/416729a, 2002.

596 Finney, B. P. et al.: Impacts of Climatic Change and Fishing on Pacific Salmon Abundance
597 Over the Past 300 Years, Science, 290, 795-799., 2000.

598 Freudenthal, T., Neuer, S., Meggers, H., Davenport, R. and Wefer, G.: Influence of lateral
599 particle advection and organic matter degradation on sediment accumulation and stable
600 nitrogen isotope ratios along a productivity gradient in the Canary Islands region, Mar.
601 Geol., 17, 2001.

602 Fripiat, F., Declercq, M., Sapart, C. J., Anderson, L. G., Bruechert, V., Deman, F., Fonseca-
603 Batista, D., Humborg, C., Roukaerts, A., Semiletov, I. P. and Dehairs, F.: Influence of the
604 bordering shelves on nutrient distribution in the Arctic halocline inferred from water
605 column nitrate isotopes, Limnol. Oceanogr., 63(5), 2018.

606 Galbraith, E. D.: Interactions between climate and the marine nitrogen cycle on glacial-
607 interglacial timescales, University of British Columbia, Vancouver., 2007.

608 Garcia, H. E., Locarnini, T. P., Boyer, T. P., Antonov, J. I., Zweng, M. M., Baranova, O. K. and
609 Johnson, D. R.: Volume 4: Nutrients (phosphate, nitrate, and silicate), in World Ocean Atlas
610 2009, pp. 1–44, U.S. Government Printing Office., 2010.

611 Gaye, B., Nagel, B., Dähnke, K., Rixen, T. and Emeis, K.-C.: Evidence of parallel denitrification
612 and nitrite oxidation in the ODZ of the Arabian Sea from paired stable isotopes of nitrate
613 and nitrite, Glob. Biogeochem. Cycles, 27(4), 1059–1071, doi:10.1002/2011GB004115,
614 2013.

615 Graham, B. S., Grubbs, D., Holland, K. and Popp, B. N.: A rapid ontogenetic shift in the diet of
616 juvenile yellowfin tuna from Hawaii, Mar. Biol., 150(4), 647–658, doi:10.1007/s00227-006-
617 0360-y, 2007.

618 Granger, J., Prokopenko, M. G., Sigman, D. M., Mordy, C. W., Morse, Z. M., Morales, L. V.,
619 Sambrotto, R. N. and Plessen, B.: Coupled nitrification-denitrification in sediment of the
620 eastern Bering Sea shelf leads to (15)N enrichment of fixed N in shelf waters, J. Geophys.
621 Res.-Oceans, 116, doi:10.1029/2010jc006751, 2011.

622 Granger, J., Prokopenko, M. G., Mordy, C. W. and Sigman, D. M.: The proportion of
623 remineralized nitrate on the ice-covered eastern Bering Sea shelf evidenced from the
624 oxygen isotope ratio of nitrate, Glob. Biogeochem. Cycles, 27(3), 962–971,
625 doi:10.1002/gbc.20075, 2013.

626 Herraiz-Borreguero, L. and Rintoul, S. R.: Subantarctic mode water: distribution and
627 circulation, Ocean Dyn., 61(1), 103–126, doi:10.1007/s10236-010-0352-9, 2011.

628 Hoering, T. C. and Ford, H. T.: The isotope effect in the fixation of nitrogen by azotobacter, J.
629 Am. Chem. Soc., 82(2), 376–378, doi:10.1021/ja01487a031, 1960.

630 Holmes, E., Lavik, G., Fischer, G., Segl, M., Ruhland, G. and Wefer, G.: Seasonal variability of
631 d15N in sinking particles in the Benguela upwelling region, , 18, 2002.

632 Karsh, K. L., Trull, T. W., Lourey, A. J. and Sigman, D. M.: Relationship of nitrogen isotope
633 fractionation to phytoplankton size and iron availability during the Southern Ocean Iron
634 RElease Experiment (SOIREE), Limnol. Oceanogr., 48(3), 1058–1068, 2003.

635 Kemeny, P. C., Weigand, M. A., Zhang, R., Carter, B. R., Karsh, K. L., Fawcett, S. E. and Sigman,
636 D. M.: Enzyme-level interconversion of nitrate and nitrite in the fall mixed layer of the
637 Antarctic Ocean: Antarctic Fall Nitrate Isotopes, Glob. Biogeochem. Cycles, 30(7), 1069–
638 1085, doi:10.1002/2015GB005350, 2016.

639 Kienast, M., Lehmann, M. F., Timmermann, A., Galbraith, E., Bolliet, T., Holboum, A.,
640 Normandeau, C. and Laj, C.: A mid-Holocene transition in the nitrogen dynamics of the
641 western equatorial Pacific: Evidence of a deepening thermocline?, Geophys. Res. Lett.,
642 35(23), doi:10.1029/2008gl035464, 2008.

643 Knapp, A. N., Sigman, D. M. and Lipschultz, F.: N isotopic composition of dissolved organic
644 nitrogen and nitrate at the Bermuda Atlantic time-series study site, Glob. Biogeochem.
645 Cycles, 19(1), doi:10.1029/2004gb002320, 2005.

646 Knapp, A. N., DiFiore, P. J., Deutsch, C., Sigman, D. M. and Lipschultz, F.: Nitrate isotopic
647 composition between Bermuda and Puerto Rico: Implications for N(2) fixation in the
648 Atlantic Ocean, Glob. Biogeochem. Cycles, 22(3), doi:10.1029/2007gb003107, 2008.

649 Knapp, A. N., Sigman, D. M., Lipschultz, F., Kustka, A. B. and Capone, D. G.: Interbasin isotopic
650 correspondence between upper-ocean bulk DON and subsurface nitrate and its
651 implications for marine nitrogen cycling, Glob. Biogeochem. Cycles, 25,
652 doi:10.1029/2010gb003878, 2011.

653 Knapp, A. N., Casciotti, K. L., Berelson, W. M., Prokopenko, M. G. and Capone, D. G.: Low rates
654 of nitrogen fixation in eastern tropical South Pacific surface waters, Proc. Natl. Acad. Sci.,
655 113(16), 4398–4403, doi:10.1073/pnas.1515641113, 2016.

656 Ko, Y. H., Lee, K., Takahashi, T., Karl, D. M., Kang, S.-H. and Lee, E.: Carbon-Based Estimate of
657 Nitrogen Fixation-Derived Net Community Production in N-Depleted Ocean Gyres, Glob.
658 Biogeochem. Cycles, doi:10.1029/2017GB005634, 2018.

659 Lavik, G.: Nitrogen isotopes of sinking matter and sediments in the South Atlantic,
660 Universität Bremen, Bremen, Deutschland., 2000.

Lehmann, M. F., Sigman, D. M., McCorkle, D. C., Brunelle, B. G., Hoffmann, S., Kienast, M., Cane, G. and Clement, J.: Origin of the deep Bering Sea nitrate deficit: Constraints from the nitrogen and oxygen isotopic composition of water column nitrate and benthic nitrate fluxes, Glob. Biogeochem. Cycles, 19(4), doi:10.1029/2005gb002508, 2005.

Lehmann, N., Granger, J., Kienast, M., Brown, K. S., Rafter, P. A., Martínez-Méndez, G. and Mohtadi, M.: Isotopic Evidence for the Evolution of Subsurface Nitrate in the Western Equatorial Pacific, J. Geophys. Res. Oceans, doi:10.1002/2017JC013527, 2018.

Liu, K. K.: Geochemistry of inorganic nitrogen compounds in two marine environments: The Santa Barbara Basin and the ocean off Peru, University of Southern California, Los Angeles., 1979.

Liu, K. K., Su, M. J., Hsueh, C. R. and Gong, G. C.: The nitrogen isotopic composition of nitrate in the Kuroshio Water northeast of Taiwan: Evidence for nitrogen fixation as a source of isotopically light nitrate, Mar. Chem., 54(3–4), 273–292, doi:10.1016/0304-4203(96)00034-5, 1996.

Lourey, M. J., Trull, T. W. and Sigman, D. M.: Sensitivity of delta N-15 of nitrate, surface suspended and deep sinking particulate nitrogen to seasonal nitrate depletion in the Southern Ocean, Glob. Biogeochem. Cycles, 17(3), doi:10.1029/2002gb001973, 2003.

Marconi, D., Alexandra Weigand, M., Rafter, P. A., McIlvin, M. R., Forbes, M., Casciotti, K. L. and Sigman, D. M.: Nitrate isotope distributions on the US GEOTRACES North Atlantic cross-basin section: Signals of polar nitrate sources and low latitude nitrogen cycling, Mar. Chem., 177, 143–156, doi:10.1016/j.marchem.2015.06.007, 2015.

Marconi, D., Sigman, D. M., Casciotti, K. L., Campbell, E. C., Alexandra Weigand, M., Fawcett, S. E., Knapp, A. N., Rafter, P. A., Ward, B. B. and Haug, G. H.: Tropical Dominance of N2 Fixation in the North Atlantic Ocean: Tropical Lead of Atlantic N2 fixation, Glob. Biogeochem. Cycles, 31(10), 1608–1623, doi:10.1002/2016GB005613, 2017.

Mariotti, A., Germon, J. C., Hubert, P., Kaiser, P., Letolle, R., Tardieux, A. and Tardieux, P.: Experimental determination of nitrogen kinetic isotope fractionation—some principles—illustration for the denitrification and nitrification processes, Plant Soil, 62(3), 413–430, 1981.

Marquardt, D. W.: An Algorithm for Least-Squares Estimation of Nonlinear Parameters, J. Soc. Ind. Appl. Math., 11(2), 431–441, doi:10.1137/0111030, 1963.

Martin, T. S. and Casciotti, K. L.: Paired N and O isotopic analysis of nitrate and nitrite in the Arabian Sea oxygen deficient zone, Deep Sea Res. Part Oceanogr. Res. Pap., 121, 121–131, doi:10.1016/j.dsr.2017.01.002, 2017.

Miyake, Y. and Wada, E.: The Abundance Ratio of 15N/14N in Marine Environments, Rec. Oceanogr. Works Jpn., 9(l), 1967.

697 Palter, J. B., Sarmiento, J. L., Gnanadesikan, A., Simeon, J. and Slater, R. D.: Fueling export
698 production: nutrient return pathways from the deep ocean and their dependence on the
699 Meridional Overturning Circulation, Biogeosciences, 7(11), 3549–3568, doi:10.5194/bg-7-
700 3549-2010, 2010.

701 Pantoja, S., Repeta, D. J., Sachs, J. P. and Sigman, D. M.: Stable isotope constraints on the
702 nitrogen cycle of the Mediterranean Sea water column, Deep-Sea Res. Part -Oceanogr. Res.
703 Pap., 49(9), 1609–1621, doi:10.1016/s0967-0637(02)00066-3, 2002.

704 Peters, B. D., Lam, P. J. and Casciotti, K. L.: Nitrogen and oxygen isotope measurements of
705 nitrate along the US GEOTRACES Eastern Pacific Zonal Transect (GP16) yield insights into
706 nitrate supply, remineralization, and water mass transport, Mar. Chem.,
707 doi:10.1016/j.marchem.2017.09.009, 2017.

708 Rafter, P. A. and Charles, C. D.: Pleistocene equatorial Pacific dynamics inferred from the
709 zonal asymmetry in sedimentary nitrogen isotopes, Paleoceanography, 27,
710 doi:10.1029/2012pa002367, 2012.

711 Rafter, P. A. and Sigman, D. M.: Spatial distribution and temporal variation of nitrate
712 nitrogen and oxygen isotopes in the upper equatorial Pacific Ocean, Limnol. Oceanogr.,
713 61(1), 14–31, doi:10.1002/lno.10152, 2016.

714 Rafter, P. A., Sigman, D. M., Charles, C. D., Kaiser, J. and Haug, G. H.: Subsurface tropical
715 Pacific nitrogen isotopic composition of nitrate: Biogeochemical signals and their transport,
716 Glob. Biogeochem. Cycles, 26, doi:10.1029/2010gb003979, 2012.

717 Rafter, P. A., DiFiore, P. J. and Sigman, D. M.: Coupled nitrate nitrogen and oxygen isotopes
718 and organic matter remineralization in the Southern and Pacific Oceans, J. Geophys. Res.
719 Oceans, 118, 1–14, doi:10.1002/jgrc.20316, 2013.

720 Ren, H., Sigman, D. M., Meckler, A. N., Plessen, B., Robinson, R. S., Rosenthal, Y. and Haug, G.
721 H.: Foraminiferal Isotope Evidence of Reduced Nitrogen Fixation in the Ice Age Atlantic
722 Ocean, Science, 323(5911), 244–248, doi:10.1126/science.1165787, 2009.

723 Ren, H., Chen, Y.-C., Wang, X. T., Wong, G. T. F., Cohen, A. L., DeCarlo, T. M., Weigand, M. A.,
724 Mii, H.-S. and Sigman, D. M.: 21st-century rise in anthropogenic nitrogen deposition on a
725 remote coral reef, Science, 356(6339), 749–752, doi:10.1126/science.aal3869, 2017.

726 Robinson, R. S., Brunelle, B. G. and Sigman, D. M.: Revisiting nutrient utilization in the glacial
727 Antarctic: Evidence from a new method for diatom-bound N isotopic analysis,
728 Paleoceanography, 19(3), doi:10.1029/2003pa000996, 2004.

729 Robinson, R. S., Kienast, M., Albuquerque, A. L., Altabet, M., Contreras, S., Holz, R. D., Dubois,
730 N., Francois, R., Galbraith, E., Hsu, T. C., Ivanochko, T., Jaccard, S., Kao, S. J., Kiefer, T., Kienast,
731 S., Lehmann, M. F., Martinez, P., McCarthy, M., Mobius, J., Pedersen, T., Quan, T. M.,
732 Ryabenko, E., Schmittner, A., Schneider, R., Schneider-Mor, A., Shigemitsu, M., Sinclair, D.,

733 Somes, C., Studer, A., Thunell, R. and Yang, J. Y.: A review of nitrogen isotopic alteration in
734 marine sediments, Paleoceanography, 27, doi:10.1029/2012pa002321, 2012.

735 Rumelhart, D. E., Hinton, G. E. and Williams, R. J.: Learning Representations by Back-
736 Propagating Errors, Nature, 323(6088), 533–536, doi:10.1038/323533a0, 1986.

737 Ryabenko, E., Kock, A., Bange, H. W., Altabet, M. A. and Wallace, D. W. R.: Contrasting
738 biogeochemistry of nitrogen in the Atlantic and Pacific Oxygen Minimum Zones,
739 Biogeosciences, 9(1), 203–215, doi:10.5194/bg-9-203-2012, 2012.

740 Sachs, J. P., Repeta D. J.: Oligotrophy and nitrogen fixation during eastern Mediterranean
741 sapropel events, Science, 286(5449), 2485–2488, 1999.

742 Sarmiento, J. L., Gruber, N., Brzezinski, M. A. and Dunne, J. P.: High-latitude controls of
743 thermocline nutrients and low latitude biological productivity, Nature, 427(6969), 56–60,
744 doi:10.1038/nature02127, 2004.

745 Schlitzer, R.: Ocean Data View. [online] Available from: http://www.awi-
746 bremerhaven.de/GEO/ODV, 2002.

747 Schlitzer, R., Anderson, R. F., Dodas, E. M., Lohan, M., Geibert, W., Tagliabue, A., Bowie, A.,
748 Jeandel, C., Maldonado, M. T., Landing, W. M., Cockwell, D., Abadie, C., Abouchami, W.,
749 Achterberg, E. P., Agather, A., Aguliar-Islas, A., van Aken, H. M., Andersen, M., Archer, C.,
750 Auro, M., de Baar, H. J., Baars, O., Baker, A. R., Bakker, K., Basak, C., Baskaran, M., Bates, N. R.,
751 Bauch, D., van Beek, P., Behrens, M. K., Black, E., Bluhm, K., Bopp, L., Bouman, H., Bowman,
752 K., Bown, J., Boyd, P., Boye, M., Boyle, E. A., Branellec, P., Bridgestock, L., Brissebrat, G.,
753 Browning, T., Bruland, K. W., Brumsack, H.-J., Brzezinski, M., Buck, C. S., Buck, K. N.,
754 Buesseler, K., Bull, A., Butler, E., Cai, P., Mor, P. C., Cardinal, D., Carlson, C., Carrasco, G.,
755 Casacuberta, N., Casciotti, K. L., Castrillejo, M., Chamizo, E., Chance, R., Charette, M. A.,
756 Chaves, J. E., Cheng, H., Chever, F., Christl, M., Church, T. M., Closset, I., Colman, A., Conway,
757 T. M., Cossa, D., Croot, P., Cullen, J. T., Cutter, G. A., Daniels, C., Dehairs, F., Deng, F., Dieu, H.
758 T., Duggan, B., Dulaquais, G., Dumousseaud, C., Echegoyen-Sanz, Y., Edwards, R. L., Ellwood,
759 M., Fahrbach, E., Fitzsimmons, J. N., Russell Flegal, A., Fleisher, M. Q., van de Flierdt, T.,
760 Frank, M., Friedrich, J., Fripiat, F., Fröllje, H., Galer, S. J. G., Gamo, T., Ganeshram, R. S., Garcia-
761 Orellana, J., Garcia-Solsona, E., Gault-Ringold, M., et al.: The GEOTRACES Intermediate Data
762 Product 2017, Chem. Geol., doi:10.1016/j.chemgeo.2018.05.040, 2018.

763 Sigman, D. M. and Casciotti, K. L.: Nitrogen Isotopes in the Ocean, in Encyclopedia of Ocean
764 Science, pp. 1884–1894, Academic Press., 2001.

765 Sigman, D. M., Altabet, M. A., McCorkle, D. C., Francois, R. and Fischer, G.: The delta N-15 of
766 nitrate in the Southern Ocean: Consumption of nitrate in surface waters, Glob. Biogeochem.
767 Cycles, 13(4), 1149–1166, 1999a.

768 Sigman, D. M., Altabet, M. A., Francois, R., McCorkle, D. C. and Gaillard, J. F.: The isotopic
769 composition of diatom-bound nitrogen in Southern Ocean sediments, Paleoceanography,
770 14(2), 118–134, 1999b.

771 Sigman, D. M., Granger, J., DiFiore, P. J., Lehmann, M. M., Ho, R., Cane, G. and van Geen, A.:
772 Coupled nitrogen and oxygen isotope measurements of nitrate along the eastern North
773 Pacific margin, Glob. Biogeochem. Cycles, 19(4), doi:10.1029/2005gb002458, 2005.

774 Sigman, D. M., DiFiore, P. J., Hain, M. P., Deutsch, C. and Karl, D. M.: Sinking organic matter
775 spreads the nitrogen isotope signal of pelagic denitrification in the North Pacific, Geophys.
776 Res. Lett., 36, doi:10.1029/2008gl035784, 2009a.

777 Sigman, D. M., DiFiore, P. J., Hain, M. P., Deutsch, C., Wang, Y., Karl, D. M., Knapp, A. N.,
778 Lehmann, M. F. and Pantoja, S.: The dual isotopes of deep nitrate as a constraint on the
779 cycle and budget of oceanic fixed nitrogen, Deep-Sea Res. Part -Oceanogr. Res. Pap., 56(9),
780 1419–1439, doi:10.1016/j.dsr.2009.04.007, 2009b.

781 Smart, S. M., Fawcett, S. E., Thomalla, S. J., Weigand, M. A., Reason, C. J. C. and Sigman, D. M.:
782 Isotopic evidence for nitrification in the Antarctic winter mixed layer, Glob. Biogeochem.
783 Cycles, 29(4), 427–445, doi:10.1002/2014GB005013, 2015.

784 Somes, C. J., Schmittner, A. and Altabet, M. A.: Nitrogen isotope simulations show the
785 importance of atmospheric iron deposition for nitrogen fixation across the Pacific Ocean,
786 Geophys. Res. Lett., 37, doi:10.1029/2010gl044537, 2010.

787 Tawa, A., Ishihara, T., Uematsu, Y., Ono, T. and Ohshimo, S.: Evidence of westward
788 transoceanic migration of Pacific bluefin tuna in the Sea of Japan based on stable isotope
789 analysis, Mar. Biol., 164(4), doi:10.1007/s00227-017-3127-8, 2017.

790 Thimm, G. and Fiesler, E.: Optimal Setting of Weights, Learning Rate, and Gain, , 15, 1997.

791 Thunell, R. C., Sigman, D. M., Muller-Karger, F., Astor, Y. and Varela, R.: Nitrogen isotope
792 dynamics of the Cariaco Basin, Venezuela, Glob. Biogeochem. Cycles, 18(3),
793 doi:10.1029/2003gb002185, 2004.

794 Toggweiler, J. R. and Carson, S.: What Are Upwelling Systems Contributing to the Ocean's
795 Carbon and Nutrient Budgets?, in Upwellmg in the Ocean: Modern Processes and Ancient
796 Records, edited by K.-C. . meis C.P. Summerhayes M. V. Angel, R. L. Smith, and B. Zeiizschcl,
797 John Wiley & Sons Ltd., 1995.

798 Toggweiler, J. R., Dixon, K. and Broecker, W. S.: The Peru upwelling and the ventilation of
799 the South-Pacific thermocline, J. Geophys. Res.-Oceans, 96(C11), 20467–20497,
800 doi:10.1029/91jc02063, 1991.

801 Trull, T. W., Davies, D. and Casciotti, K.: Insights into nutrient assimilation and export in
802 naturally iron-fertilized waters of the Southern Ocean from nitrogen, carbon and oxygen
803 isotopes, Deep Sea Res. Part II Top. Stud. Oceanogr., 55(5–7), 820–840,
804 doi:10.1016/j.dsr2.2007.12.035, 2008.

805 Tuerena, R. E., Ganeshram, R. S., Geibert, W., Fallick, A. E., Dougans, J., Tait, A., Henley, S. F.
806 and Woodward, E. M. S.: Nutrient cycling in the Atlantic basin: The evolution of nitrate

807 isotope signatures in water masses, Glob. Biogeochem. Cycles, 29(10), 1830–1844,
808 doi:10.1002/2015GB005164, 2015.

809 Umezawa, Y., Yamaguchi, A., Ishizaka, J., Hasegawa, T., Yoshimizu, C., Tayasu, I., Yoshimura,
810 H., Morii, Y., Aoshima, T. and Yamawaki, N.: Seasonal shifts in the contributions of the
811 Changjiang River and the Kuroshio Current to nitrate dynamics in the continental shelf of
812 the northern East China Sea based on a nitrate dual isotopic composition approach,
813 Biogeosciences, 11(4), 1297–1317, doi:10.5194/bg-11-1297-2014, 2014.

814 Voss, M.: Räumliche und zeitliche Verteilung stabiler Isotope (d15N, d13C) in
815 suspendierten und sedimentierten Partikeln im Nördlichen Nordatlantik, Christian-
816 Albrechts-Universitat zu Kiel., 1991.

817 Voss, M., Dippner, J. W. and Montoya, J. P.: Nitrogen isotope patterns in the oxygen-deficient
818 waters of the Eastern Tropical North Pacific Ocean, Deep-Sea Res. Part -Oceanogr. Res. Pap.,
819 48(8), 1905–1921, doi:10.1016/s0967-0637(00)00110-2, 2001.

820 Wada, E.: Nitrogen Isotope Fractionation and Its Significance in Biogeochemical Processes
821 Occurring in Marine Environments, in Isotope Marine Chemistry, pp. 375–398., 1980.

822 Wada, E. and Hattori, A.: Nitrogen isotope effects in the assimilation of inorganic
823 nitrogenous compounds by marine diatoms, Geomicrobiol. J., 1(1), 85–101, 1978.

824 Weigend, A. S., Huberman, B. A. and Rumelhart, D. E.: Predicting The Future: A
825 Connectionist Approach, Int. J. Neural Syst., 1(3), 193–209,
826 doi:10.1142/s0129065790000102, 1990.

827 Wong, G. T. F., Chung, S.-W., Shiah, F.-K., Chen, C.-C., Wen, L.-S. and Liu, K.-K.: Nitrate
828 anomaly in the upper nutricline in the northern South China Sea - Evidence for nitrogen
829 fixation, Geophys. Res. Lett., 29(23), 12-1-12–4, doi:10.1029/2002GL015796, 2002.

830 Wu, J., Calvert, S. E. and Wong, C. S.: Nitrogen isotope variations in the subarctic northeast
831 Pacific: relationships to nitrate utilization and trophic structure, Deep Sea Res. Part
832 Oceanogr. Res. Pap., 44(2), 287–314, 1997.

833 Yang, S. and Gruber, N.: The anthropogenic perturbation of the marine nitrogen cycle by
834 atmospheric deposition: Nitrogen cycle feedbacks and the ^{15} N Haber-Bosch effect, Glob.
835 Biogeochem. Cycles, 30(10), 1418–1440, doi:10.1002/2016GB005421, 2016.

836 Yang, S., Gruber, N., Long, M. C. and Vogt, M.: ENSO-Driven Variability of Denitrification and
837 Suboxia in the Eastern Tropical Pacific Ocean, Glob. Biogeochem. Cycles, 31(10), 1470–
838 1487, doi:10.1002/2016GB005596, 2017.

839 Yoshikawa, C., Nakatsuka, T. and Wakatsuchi, M.: Distribution of N* in the Sea of Okhotsk
840 and its use as a biogeochemical tracer of the Okhotsk Sea Intermediate Water formation
841 process, J. Mar. Syst., 63(1–2), 49–62, doi:10.1016/j.jmarsys.2006.05.008, 2006.

Yoshikawa, C., Makabe, A., Shiozaki, T., Toyoda, S., Yoshida, O., Furuya, K. and Yoshida, N.: Nitrogen isotope ratios of nitrate and N* anomalies in the subtropical South Pacific, Geochem. Geophys. Geosystems, 16(5), 1439–1448, doi:10.1002/2014GC005678, 2015.

847 **Appendix: References for this version of seawater nitrate $\delta^{15}N$ compilation**

region	year of sampling	month of sampling	reference
Pacific North – Subarctic	Unknown sampling date	*na*	(Altabet and Francois, 1994b)
Indian – Arabian Sea	1995	8	(Altabet et al., 1999)
Southern Ocean - Pacific	1996-1998	1-4,8-11	(Altabet and Francois, 2001)
Pacific North – Gulf of California	1990	6	(Altabet, 1999)
Pacific North – Subarctic	1971	7	(Wada, 1980)
Indian – Arabian Sea	1994	4	(Brandes et al., 1998)
Pacific North – ETNP	1993	12	(Brandes et al., 1998)
Pacific North - Kuroshio	1992 & 1994	3 & 4	(Liu et al., 1996)
Pacific North – Tropical	1997	10 & 11	(Voss et al., 2001)
Pacific North – Subarctic	2003	2	(Galbraith, 2007)
Atlantic North	2004	5	(Bourbonnais et al., 2009)
Mediterranean	1996	5	(Sachs, 1999)
Mediterranean	1998	1	(Pantoja et al., 2002)
Pacific North – Subarctic	2002	6	(Lehmann et al., 2005)
Pacific South – Tropical	1977	6	(Liu, 1979)
Pacific South – Tropical	2002 & 2004	4 & 5	(De Pol-Holz et al., 2009)
Pacific North – Okhotsk	1998, 1999, 2000	6 & 9	(Yoshikawa et al., 2006)
Pacific Tropical	2006	6	(Kienast et al., 2008)
Southern Ocean – Indian	2005	1 & 2	(Trull et al., 2008)
Pacific South – Tropical	2008 & 2009	1, 2, & 12	(Ryabenko et al., 2012)
Indian South	2011	10 & 11	(Dehairs et al., 2015)
Pacific South – Tropical	2012	11	(Bourbonnais et al., 2015)
Indian North	2007	9	(Gaye et al., 2013)
Atlantic South	2010 & 2012	10 & 1	(Tuerena et al., 2015)
Pacific South	2009	6	(Yoshikawa et al., 2015)

Pacific North –SCS	1997	4	(Wong et al., 2002)
Pacific North – Bering Sea	2008 & 2007	4 & 5	(Granger et al., 2011, 2013)
Arctic – Beaufort	2009	9	Granger unpublished
Atlantic North	2010	10 & 11	Jenkins et al. Unpublished GEOTRACES (Knorr_199_leg4.pdf)
Atlantic Tropical	2010	2 & 3	Frank et al. Unpublished GEOTRACES (meteor81_1.pdf)
Pacific Tropical	2013	5 & 6	(Lehmann et al., 2018)
Pacific North	2008	7	Granger Unpublished
Pacific North	2009 & 2011	2 & 7	(Umezawa et al., 2014)
Pacific South – Tropical	2010 & 2011	2-4	(Knapp et al., 2016)
Atlantic North – Subarctic	1989	6	(Voss, 1991)
Southern Ocean – Pacific	1995	4	(Sigman et al., 1999a)
Southern Ocean – Indian	1995	1	(Sigman et al., 1999a)
Southern Ocean – Pacific	2016		(Kemeny et al., 2016)
Pacific North – Tropical	2003	10	(Sigman et al., 2005)
Pacific North – ALOHA	2000	11	(Sigman et al., 2009b)
Atlantic – North	2001-2002	1-12	(Knapp et al., 2005)
Atlantic – North	2002	10	(Knapp et al., 2008)
Pacific – North	2003	7 & 8	(Knapp et al., 2011)
Indian - South	1999	1 & 2	(Karsh et al., 2003)
Southern – Indian	1998 & 1999	2,3,4,9, & 12	(DiFiore et al., 2006)
Southern – Atlantic	2012	7	(Smart et al., 2015)
Atlantic – North	2011	10 & 11	(Marconi et al., 2015)
Pacific – North ALOHA	2004	7	(Casciotti et al., 2008)
Pacific – South Tropical	2005	11	(Casciotti et al., 2013)
Pacific – North Tropical	2003	11	(Casciotti and McIlvin, 2007)
Indian – Arabian	2007	9	(Martin and Casciotti, 2017)
Pacific – Tropical	2004-2007	3-12	(Rafter et al., 2012; Rafter and Sigman, 2016)

Indian – Arabian Sea	2007	10	(DeVries et al., 2012) or Rafter and Sigman Unpublished
Pacific South – Tasman Sea	2010	1 & 2	Rafter and Sigman Unpublished
Pacific South – Tropical	2010	2	(Rafter et al., 2012)
Atlantic North – Subarctic	2010	4	Rafter and Sigman Unpublished
Pacific South	2005	1	(Rafter et al., 2013)
Pacific South – Tropical	2013	10-12	(Peters et al., 2017)
Atlantic North – Subarctic	2013	8	(Marconi et al., 2017)
Pacific North – Subarctic	1993	5	(Wu et al., 1997)
Arctic	2014	7 & 8	(Fripiat et al., 2018)

848
849

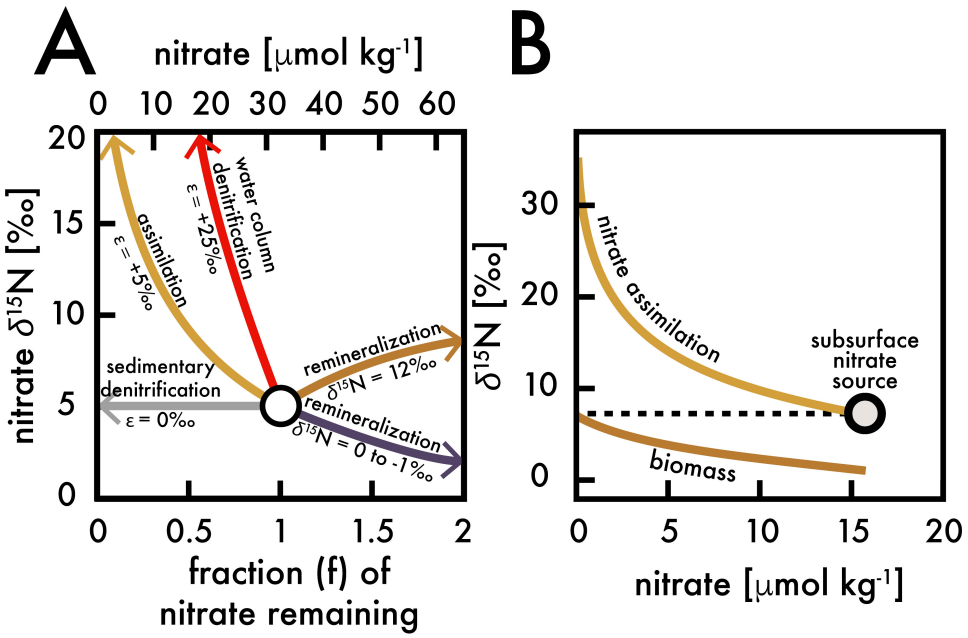

Figure 1: (A) A comparison of influences on average deep-sea nitrate (circle; concentration and $\delta^{15}N$ estimated here by EANN results in this work) including: the isotope effects of assimilation (yellow arrow), water column and sedimentary denitrification (red and gray arrows), and the addition of nitrate via remineralization of organic matter with higher and lower $\delta^{15}N$ (brown and purple arrows) (modified from Galbraith et al., (2008)). (B) An example of N isotopic fractionation on nitrate and organic matter biomass during nitrate assimilation in eastern equatorial Pacific surface waters (from Rafter and Sigman, (2016)). These calculations are based on isotopic fractionation equations of (Mariotti et al., 1981) simplified in (Sigman and Casciotti, 2001) with an isotope effect (ε) as shown in (A). The variable "f" is the observed / initial nitrate concentration.

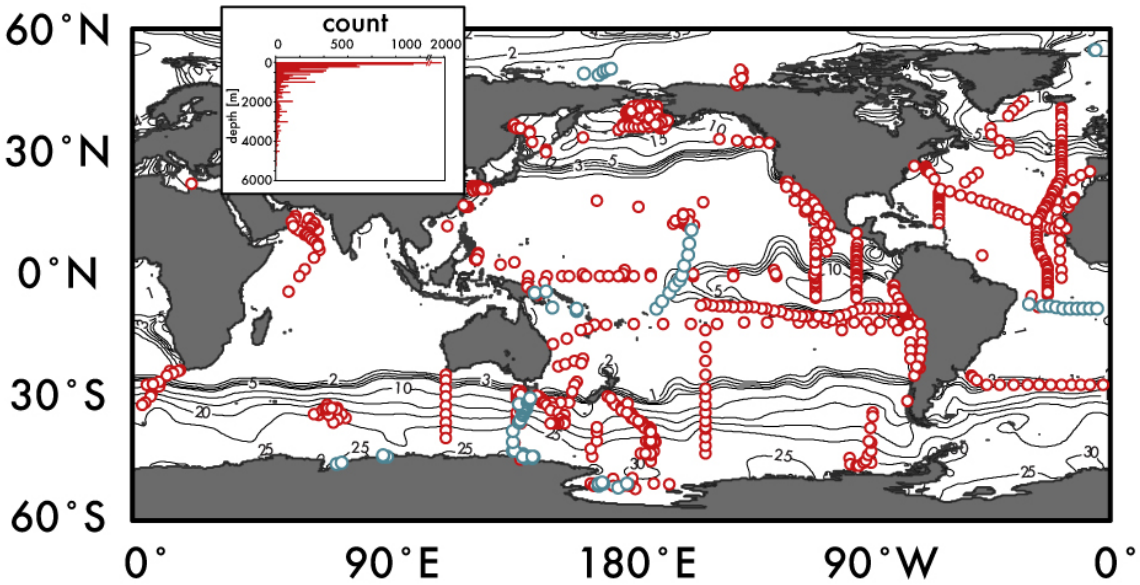

Figure 2: The location of global nitrate $\delta^{15}N$ observations used to constrain the Ensemble of Artificial Neural Networks are shown as red circles. Observations used as an 'external validation dataset' (those withheld from training the EANN) are shown in blue. Inset figure shows the number of observations versus depth. Contours are surface nitrate concentrations for October-December from World Ocean Atlas (Garcia et al., 2014).

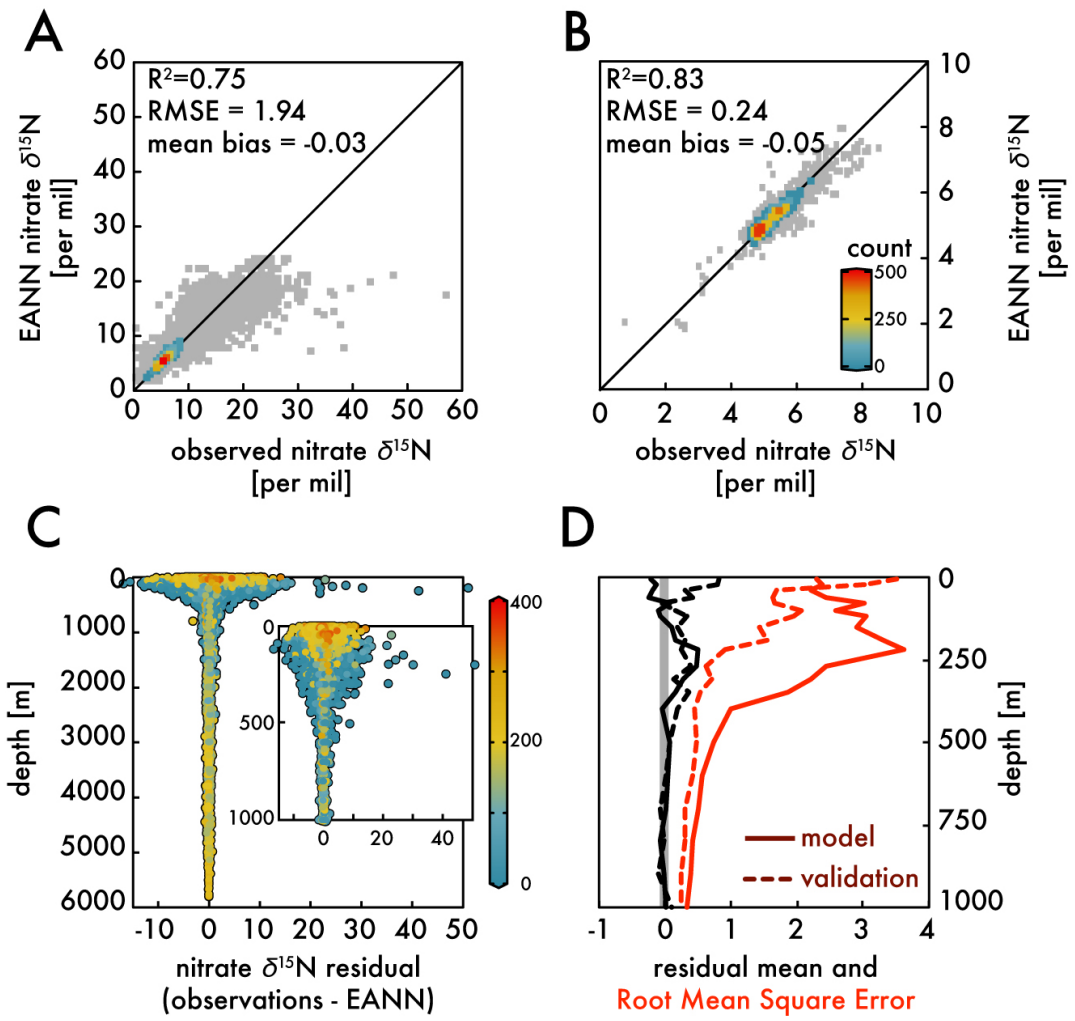

Figure 3: The binned observed versus EANN-predicted nitrate δ^{15}N are shown for all data at all depths in (A) and for >1000 m in (B). The colors indicate the number of comparisons on the World Ocean Atlas grid. The anomalously high observed nitrate δ^{15}N values (>30‰) in (A) are exclusively from the Eastern Tropical South Pacific waters (Bourbonnais et al., 2015; Casciotti et al., 2013; Rafter et al., 2012; Ryabenko et al., 2012). The difference (or residual) between the observations and EANN nitrate δ^{15}N is made for all depths and the upper 1000 m in (C) with colors representing the dissolved oxygen content. Note the largest offsets between 100-500 m in (C) are associated with lowest oxygen content. Similarly, the mean residual (black) and Root Mean Square Error (RMSE; red) with depth (D) are highest in the upper 500 m. Dashed lines in (D) demonstrate the same statistics, but for the external validation dataset (blue in Fig. 2).

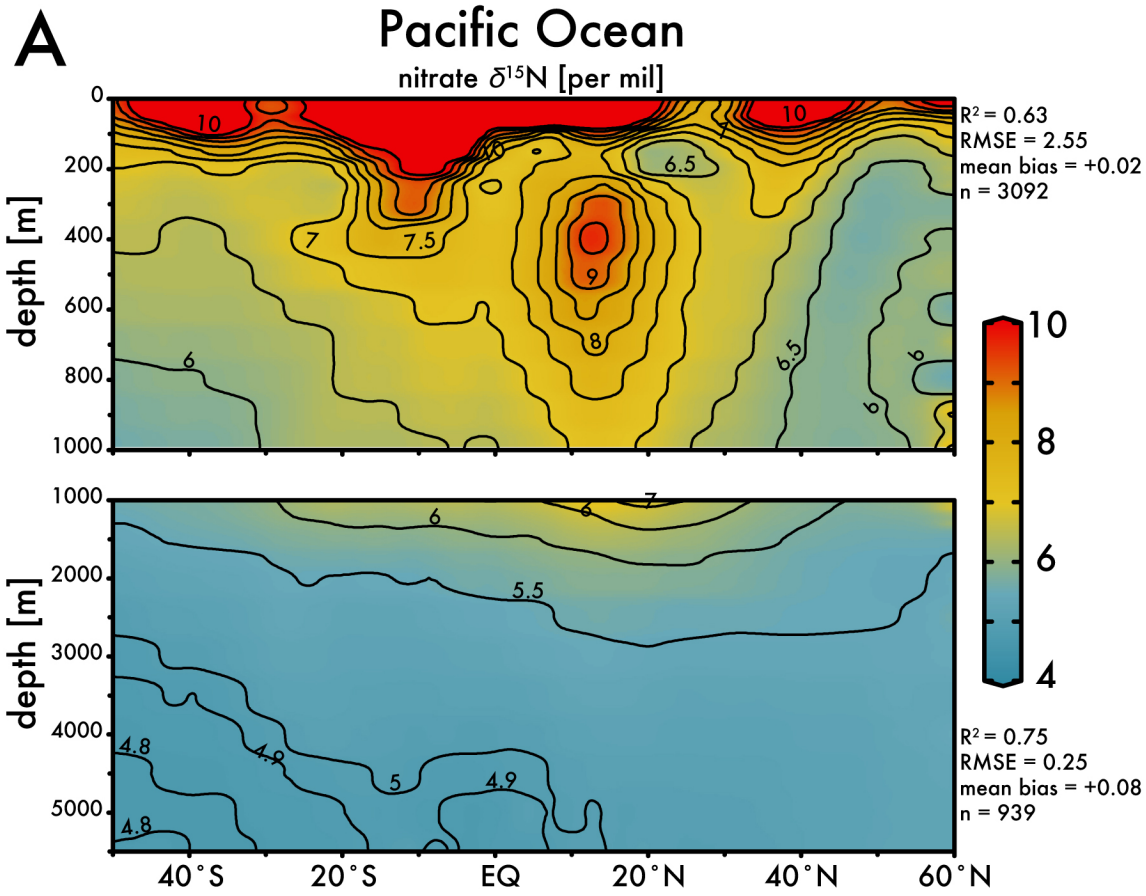
A
Pacific Ocean
nitrate δ15N [per mil]
depth [m]
0
200
400
600
800
1000
1000
2000
3000
4000
5000
10
7
7.5
6.5
9
8
6
5.5
5
4.9
4.8
40°S
20°S
EQ
20°N
40°N
60°N
R2 = 0.63
RMSE = 2.55
mean bias = +0.02
n = 3092
10
8
6
4
R2 = 0.75
RMSE = 0.25
mean bias = +0.08
n = 939

884

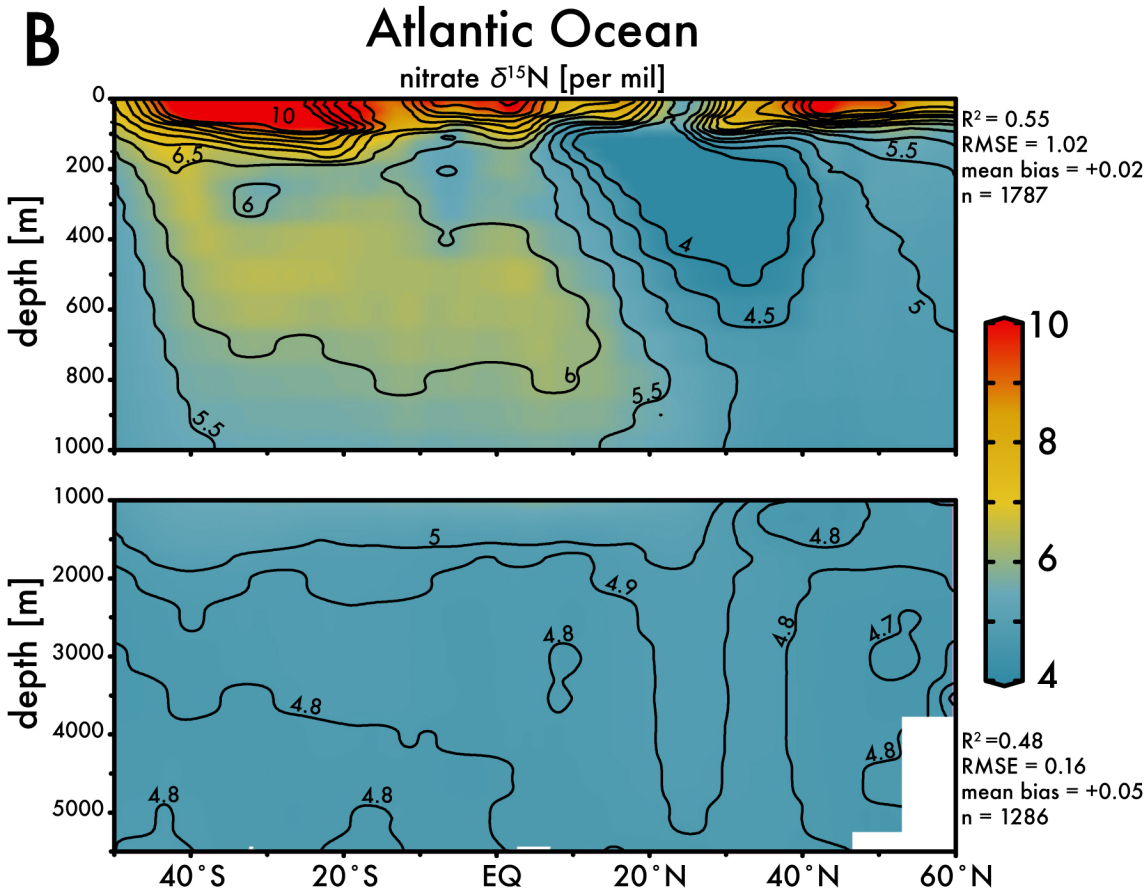
B
Atlantic Ocean
nitrate δ15N [per mil]
depth [m]
0
200
400
600
800
1000
10
6.5
6
5.5
4
4.5
5
6
5.5
5.5
R2 = 0.55
RMSE = 1.02
mean bias = +0.02
n = 1787
1000
2000
3000
4000
5000
5
4.9
4.8
4.8
4.8
4.8
4.8
4.7
4.8
4.8
10
8
6
4
R2 =0.48
RMSE = 0.16
mean bias = +0.05
n = 1286
40°S
20°S
EQ
20°N
40°N
60°N

885

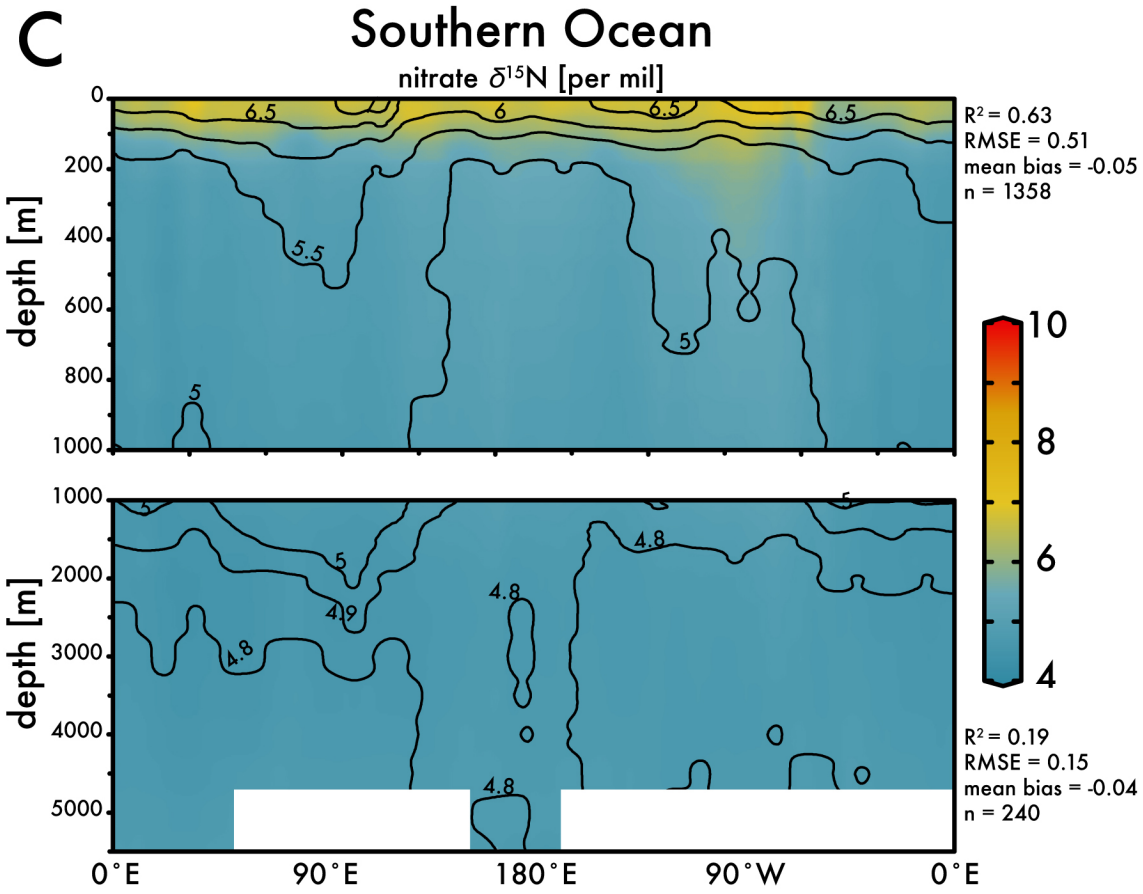
C
Southern Ocean
nitrate δ15N [per mil]
depth [m]
0
200
400
600
800
1000
2000
3000
4000
5000
6.5
6
5.5
5
4.9
4.8
0°E
90°E
180°E
90°W
0°E
R² = 0.63
RMSE = 0.51
mean bias = -0.05
n = 1358
R² = 0.19
RMSE = 0.15
mean bias = -0.04
n = 240
10
8
6
4

886
887

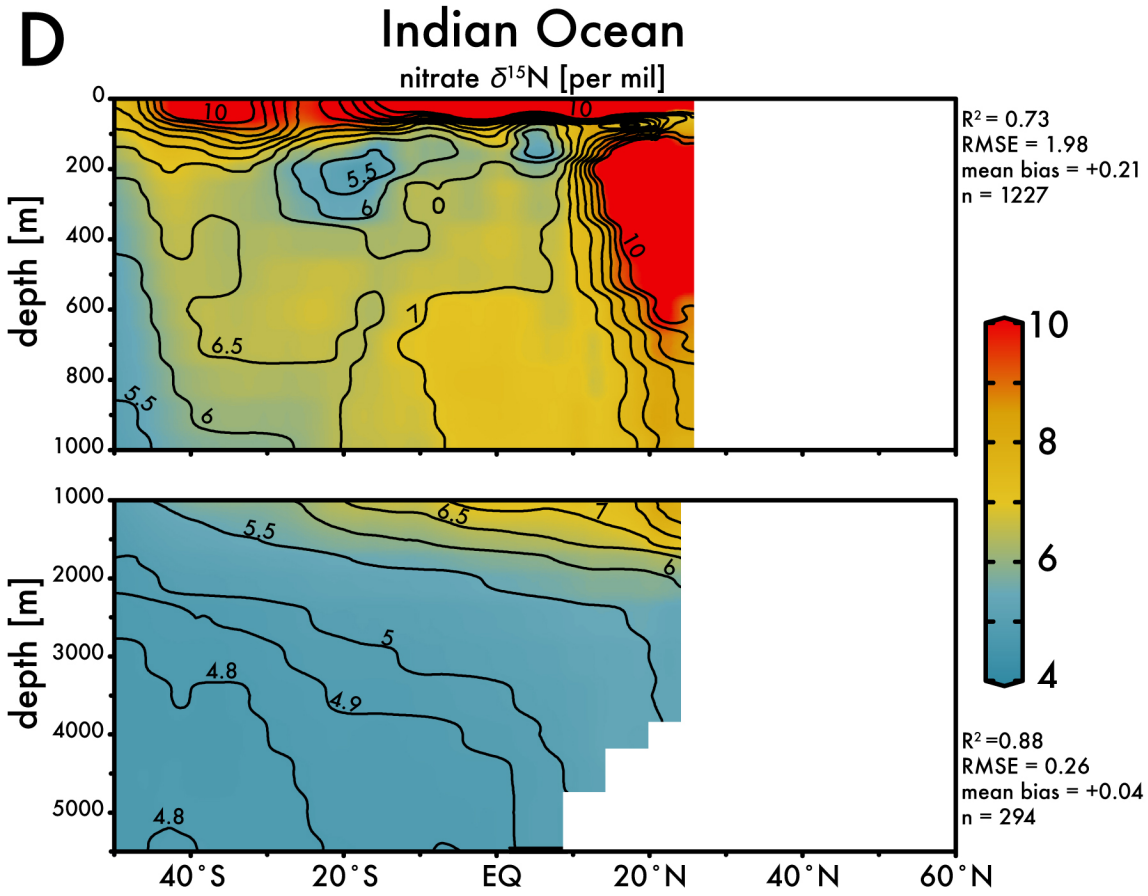

Figure 4: Zonal average of model nitrate $\delta^{15}N$ versus latitude or longitude for the: (A) Pacific Ocean, (B) Atlantic Ocean, (C) Southern Ocean, and the (D) Indian Ocean. White bars indicate no data because of land. The R^2, RMSE, mean bias, and total number (n) of observed versus EANN nitrate $\delta^{15}N$ are shown on the right for each region and depth range. White indicates regions of no data coverage. Note that these zonally-averaged views obscure zonal gradients in nitrate $\delta^{15}N$ (see Figure 5).

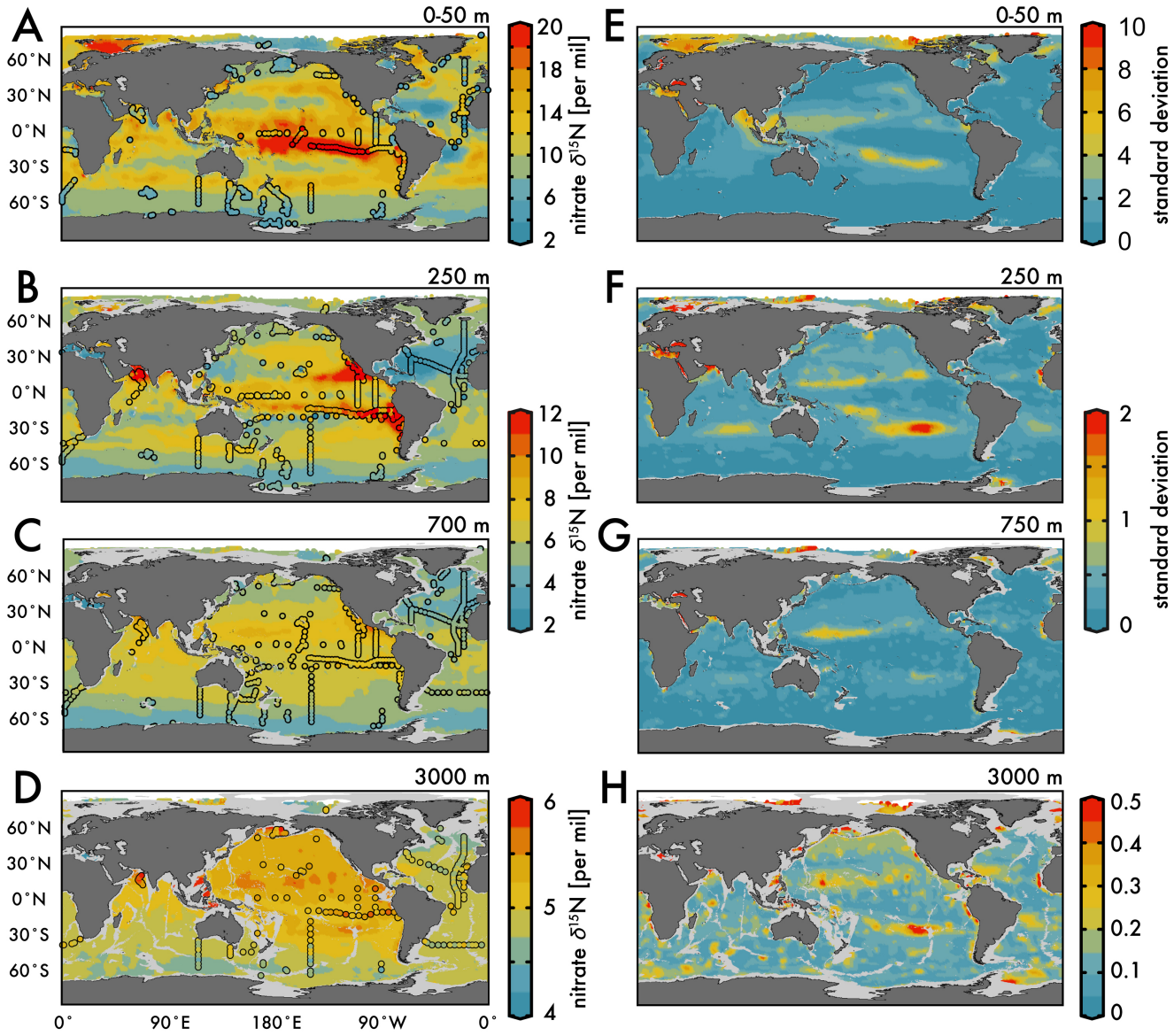

Figure 5: (Left) Map view of nitrate δ^{15}N from our EANN and our observations (circles) for the (A) average over the 0-50 m depth as well as the (B) 250 m, (C) 700 m, and (D) 3000 depth surfaces. (Right) Map views of nitrate δ^{15}N error from the EANN model nitrate δ^{15}N for the same depth surfaces on left.

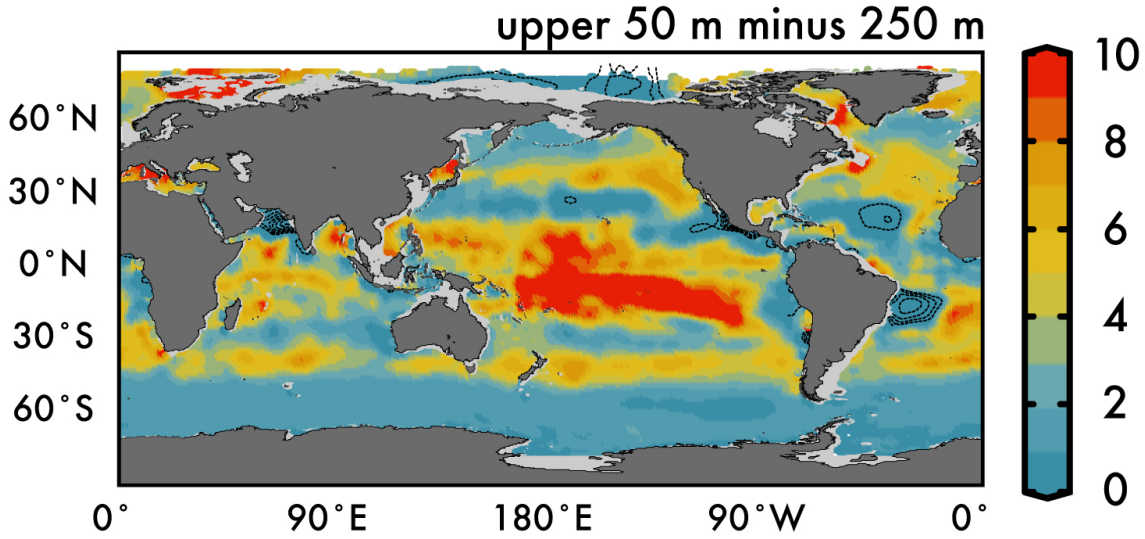

Figure 6: Difference between the average nitrate $\delta^{15}N$ in the upper 50m and 250 m depths in Figure 5. Dashed contours in low latitude ODZ regions and subtropical gyres indicate regions where nitrate $\delta^{15}N$ at 250 m is greater than the upper 50 m nitrate $\delta^{15}N$.

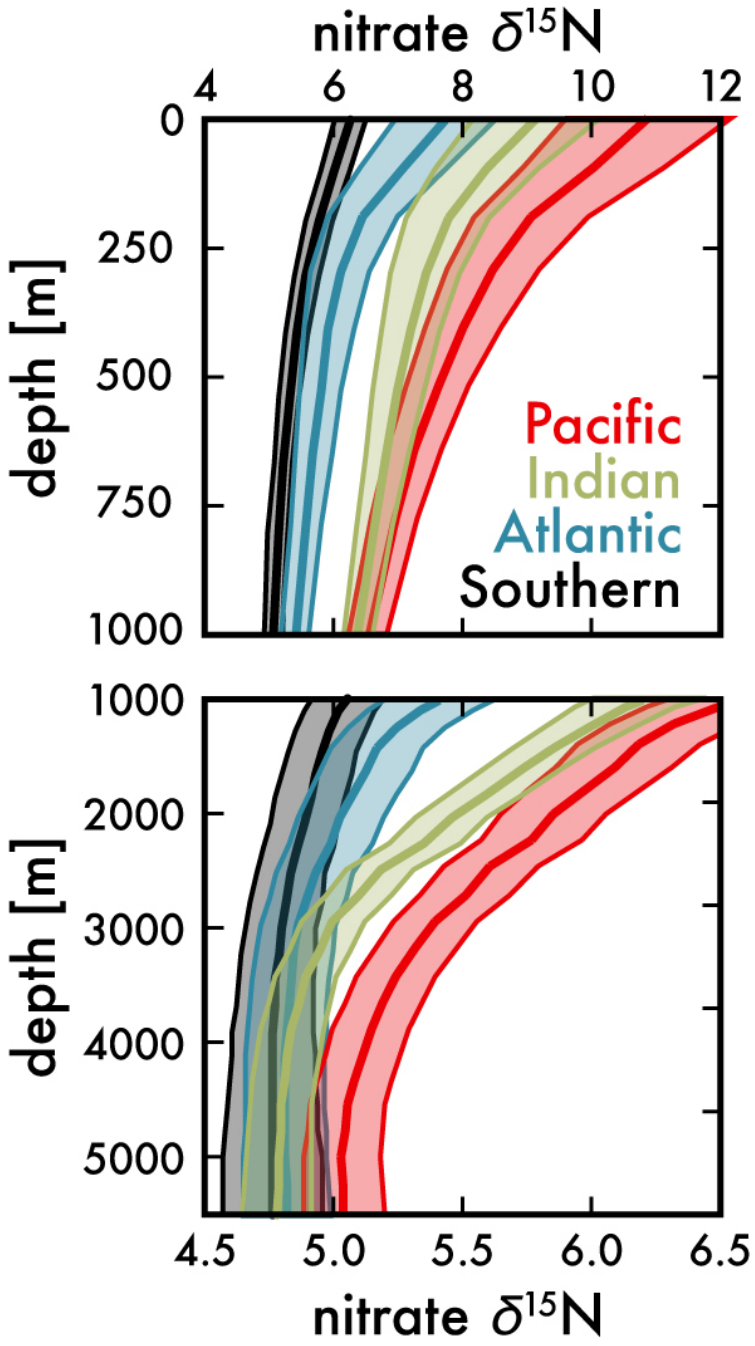

Figure 7: Mean EANN nitrate δ^{15}N (solid line) and 1-sigma standard deviation (envelope) with depth for each ocean basin. Note change in vertical and horizontal axes between top and bottom.